



NAVAL POSTGRADUATE SCHOOL

MONTEREY, CALIFORNIA

THESIS

**A MINIATURE ELECTROMECHANICAL GENERATOR
DESIGN UTILIZING HUMAN MOTION**

by

Nicholas G. Hoffman

September 2010

Thesis Co-Advisors:

Alexander L. Julian
Giovanna Oriti

Approved for public release; distribution is unlimited

THIS PAGE INTENTIONALLY LEFT BLANK

REPORT DOCUMENTATION PAGE			<i>Form Approved OMB No. 0704-0188</i>	
Public reporting burden for this collection of information is estimated to average 1 hour per response, including the time for reviewing instruction, searching existing data sources, gathering and maintaining the data needed, and completing and reviewing the collection of information. Send comments regarding this burden estimate or any other aspect of this collection of information, including suggestions for reducing this burden, to Washington headquarters Services, Directorate for Information Operations and Reports, 1215 Jefferson Davis Highway, Suite 1204, Arlington, VA 22202-4302, and to the Office of Management and Budget, Paperwork Reduction Project (0704-0188) Washington DC 20503.				
1. AGENCY USE ONLY (Leave blank)		2. REPORT DATE September 2010	3. REPORT TYPE AND DATES COVERED Master's Thesis	
4. TITLE AND SUBTITLE A Miniature Electromechanical Generator Design Utilizing Human Motion			5. FUNDING NUMBERS	
6. AUTHOR(S) Nicholas G. Hoffman				
7. PERFORMING ORGANIZATION NAME(S) AND ADDRESS(ES) Naval Postgraduate School Monterey, CA 93943-5000			8. PERFORMING ORGANIZATION REPORT NUMBER	
9. SPONSORING /MONITORING AGENCY NAME(S) AND ADDRESS(ES) N/A			10. SPONSORING/MONITORING AGENCY REPORT NUMBER	
11. SUPPLEMENTARY NOTES The views expressed in this thesis are those of the author and do not reflect the official policy or position of the Department of Defense or the U.S. Government. IRB Protocol number ____N/A____.				
12a. DISTRIBUTION / AVAILABILITY STATEMENT Approved for public release; distribution is unlimited			12b. DISTRIBUTION CODE	
13. ABSTRACT (maximum 200 words) <p>The use of Faraday's Law to design and realize a miniature electromechanical generator that converts mechanical energy from human motion into stored electrical energy was investigated in this thesis. The design incorporates simple materials composed of ferrite cores, a coil, springs and permanent magnets to convert mechanical energy provided by a user to electrical energy for storage. The generator takes advantage of a dual air-gapped electromechanical system with permanent magnets to regulate flux through a coil around a high-permeability ferrite core. Use of a compression force provided by the user reduces the air gaps in the system, causing a rapid change in flux resulting in an electromotive force that produces a current in the circuit.</p> <p>Laboratory testing of a generator prototype design verifies energy production of the mechanism and investigates the relationship between the inductance range of operation for the generator and its performance characteristics. Storage of energy produced by the generator is demonstrated using two different rectification circuits and is examined during different stages of one full stroke of the generator device. Additionally, this thesis presents a simulation that models the electromechanical energy conversion.</p>				
14. SUBJECT TERMS Generator, Mini-generator, Faraday's Law, Electromechanical, Ferromagnetic, Ferrite Core, Permanent Magnet, Electromotive Force, and Flux.			15. NUMBER OF PAGES 97	
			16. PRICE CODE	
17. SECURITY CLASSIFICATION OF REPORT Unclassified	18. SECURITY CLASSIFICATION OF THIS PAGE Unclassified	19. SECURITY CLASSIFICATION OF ABSTRACT Unclassified	20. LIMITATION OF ABSTRACT UU	

NSN 7540-01-280-5500

Standard Form 298 (Rev. 8-98)
Prescribed by ANSI Std. Z39.18

THIS PAGE INTENTIONALLY LEFT BLANK

Approved for public release; distribution is unlimited

**A MINIATURE ELECTROMECHANICAL GENERATOR DESIGN UTILIZING
HUMAN MOTION**

Nicholas G. Hoffman
Lieutenant, United States Navy
B.S., University of San Diego, 2004

Submitted in partial fulfillment of the
requirements for the degree of

MASTER OF SCIENCE IN ELECTRICAL ENGINEERING

from the

**NAVAL POSTGRADUATE SCHOOL
September 2010**

Author: Nicholas G. Hoffman

Approved by: Alexander L. Julian
Thesis Co-Advisor

Giovanna Oriti
Thesis Co-Advisor

R. Clark Robertson
Chairman, Chairman, Department of Electrical and
Computer Engineering

THIS PAGE INTENTIONALLY LEFT BLANK

ABSTRACT

The use of Faraday's Law to design and realize a miniature electromechanical generator that converts mechanical energy from human motion into stored electrical energy was investigated in this thesis. The design incorporates simple materials composed of ferrite cores, a coil, springs and permanent magnets to convert mechanical energy provided by a user to electrical energy for storage. The generator takes advantage of a dual air-gapped electromechanical system with permanent magnets to regulate flux through a coil around a high-permeability ferrite core. Use of a compression force provided by the user reduces the air gaps in the system, causing a rapid change in flux resulting in an electromotive force that produces a current in the circuit.

Laboratory testing of a generator prototype design verifies energy production of the mechanism and investigates the relationship between the inductance range of operation for the generator and its performance characteristics. Storage of energy produced by the generator is demonstrated using two different rectification circuits and is examined during different stages of one full stroke of the generator device. Additionally, this thesis presents a simulation that models the electromechanical energy conversion.

THIS PAGE INTENTIONALLY LEFT BLANK

TABLE OF CONTENTS

I.	INTRODUCTION.....	1
A.	PURPOSE.....	1
B.	MOTIVATION.....	1
C.	BACKGROUND INFORMATION.....	2
D.	APPROACH.....	5
E.	THESIS ORGANIZATION.....	6
II.	DESIGN	7
A.	INTRODUCTION.....	7
B.	THEORY OF OPERATION	7
1.	Overview.....	7
2.	Faraday's Law	7
3.	Electromechanical System	9
C.	COMPONENT SELECTION.....	15
1.	Overview.....	15
2.	Ferrite Cores	15
3.	Permanent Magnets.....	17
4.	Compression Springs	27
5.	Inductance Coil	28
6.	Electrical Energy Storage	29
D.	CHAPTER SUMMARY.....	32
III.	PERFORMANCE TESTING OF PROTOTYPE.....	33
A.	INTRODUCTION.....	33
B.	PROTOTYPE CONSTRUCTION	33
1.	Core Preparation.....	33
2.	Spring Placement	33
3.	Coil Winding.....	34
4.	Core Alignment	34
5.	Magnet Placement	34
C.	TEST RESULTS.....	35
1.	Inductance Operating Range	36
2.	Single Capacitor Storage Element	38
a.	<i>Full Stroke</i>	39
b.	<i>Compression Stage</i>	42
c.	<i>Release Stage</i>	44
3.	Half-Wave Rectifier	46
a.	<i>Compression Stage</i>	47
b.	<i>Release Stage</i>	49
4.	Doubling Circuit.....	52
a.	<i>Full-Stroke Test</i>	53
D.	CHAPTER SUMMARY.....	55
IV.	COMPUTER SIMULATION	57

A.	SIMULINK	57
B.	RESULTS.....	57
C.	CHAPTER SUMMARY.....	63
V.	CONCLUSIONS AND RECOMMENDATIONS.....	65
A.	CONCLUSION	65
B.	RECOMMENDED FURTHER RESEARCH	65
APPENDIX A. MATLAB CODE FOR INDUCTANCE PROFILE GENERATION ...		67
APPENDIX B. MATLAB CODE FOR DATA ANALYSIS		69
APPENDIX C. SIMULINK MODEL.....		71
APPENDIX D. MATLAB CODE FOR SIMULATION DATA		73
LIST OF REFERENCES.....		75
INITIAL DISTRIBUTION LIST		77

LIST OF FIGURES

Figure 1.	Three Miniaturized Generator Design Topologies: (a) Rotational, (b) Oscillatory, and (c) Hybrid. From [4].....	3
Figure 2.	Stationary Wire Loop in a Changing Magnetic Field. From [10].	8
Figure 3.	Block Diagram of Electromechanical System. After [11].....	9
Figure 4.	Energy Balance of Generator System. From [11].....	10
Figure 5.	Electromechanical System Diagram. After [11]	11
Figure 6.	Split Planar Ferrite Core. From [12].....	16
Figure 7.	Planar Ferrite Cores in Protective Case. From [13].....	16
Figure 8.	Ferrite Cores in the EM System Diagram. After [11].....	17
Figure 9.	Permanent Magnet Position in the EM System Diagram. After [11] ...	18
Figure 10.	Flux Path Through Ferrite Core.....	20
Figure 11.	Magnetization Direction Through Thickness. From [15]	20
Figure 12.	Grade N42 Nd-Fe-B Magnet Used in the Generator. From [16]	21
Figure 13.	Circuit Model With Magnet Modeled as a Flux Source and Parallel Reluctance. From [17]	22
Figure 14.	Permanent Block Magnet in Free Space. From [19].....	23
Figure 15.	Magnetic Circuit Representation of EM System With (a) Large x and R_l and (b) Small x and R_l	24
Figure 16.	Thevenin Equivalent Circuit Model of a Magnet. From [17].....	25
Figure 17.	Equivalent Magnetic Circuit for EM System.....	26
Figure 18.	Generator With Springs Positioned Close to the Magnets.....	28
Figure 19.	Compressed Generator With Coil Area Limitations	29
Figure 20.	Half-Wave Rectifier Circuit	30
Figure 21.	Voltage Doubling Circuit.....	31
Figure 22.	Miniature Generator Prototype.	35
Figure 23.	General Test Equipment Setup	36
Figure 24.	Inductance vs. Generator Displacement.....	37
Figure 25.	Single Capacitor Storage Test Circuit.....	39
Figure 26.	Full-Stroke Voltage and Current Generated Across Capacitor Terminals.....	40
Figure 27.	Full-Stroke Power Generated Across Capacitor Terminals.	41
Figure 28.	Full-Stroke Energy Generated Across Capacitor Terminals.	41
Figure 29.	Compression Stage Voltage and Current Generated Across Capacitor Terminals.	42
Figure 30.	Compression Stage Power Generated Across Capacitor Terminals..	43
Figure 31.	Compression Stage Energy Generated Across Capacitor Terminals.....	43
Figure 32.	Release Stage Voltage and Current Generated Across Capacitor Terminals.....	44
Figure 33.	Release Stage Power Generated Across Capacitor Terminals.	45
Figure 34.	Release Stage Energy Generated Across Capacitor Terminals.....	46
Figure 35.	Half-Wave Rectifier Test Circuit Setup.	47

Figure 36.	Compression Stage Voltage and Current Generated Across Capacitor Terminals.	48
Figure 37.	Compression Stage Power Generated Across Capacitor Terminals.	49
Figure 38.	Compression Stage Energy Generated Across Capacitor Terminals.	49
Figure 39.	Release Stage Voltage and Current Generated Across Capacitor Terminals.	50
Figure 40.	Release Stage Power Generated Across Capacitor Terminals.	51
Figure 41.	Release Stage Energy Generated Across Capacitor Terminals.	51
Figure 42.	Doubling Circuit Test Configuration	53
Figure 43.	Full-Stroke Voltage and Current Generated Across Both Capacitors.	54
Figure 44.	Full-Stroke Power Generated Across Both Capacitors.	54
Figure 45.	Full-Stroke Energy Generated Across Both Capacitors.	55
Figure 46.	Computer Simulated Force, Displacement and Inductance.	58
Figure 47.	Simulated Voltage and Current Response.	59
Figure 48.	Simulated Voltage and Current Data During Compression Stage.	60
Figure 49.	Simulated Voltage and Current Data During Release Stage.	61
Figure 50.	Simulated Power Generation During Full-Stroke.	62
Figure 51.	Simulated Energy During Full Stroke.	63

EXECUTIVE SUMMARY

The research completed in this thesis investigates the use of Faraday's Law to design and realize a miniature electromechanical generator that transfers mechanical energy from human motion to stored electrical energy. The continued development of low power electronics for commercial and military use has opened more opportunities for viable alternative energy sources. This thesis aims at designing such a device and proving its functionality through experimental testing of a prototype. Additionally, this thesis presents a simulation that models the electromechanical energy conversion.

The theory behind the operation of the device is based on Faraday's law, which concludes that current can be induced in closed wire loop if subjected to a time changing magnetic flux linking the surface area of the loop. From this basic principle an electromechanical system representation of a generator design was developed. The design utilizes a magnetic coupling field as a means of energy transfer and permanent magnets as the primary source of magnetic flux in the system. An inductance coil is implemented to store magnetic energy and provides the closed loop path for electric current to be flow. The electromotive force induced in the coil is proportional to the time changing flux in the system and in order to achieve a greater change in flux in relation to the displacement of the system a dual air gapped design feature was incorporated. Use of a compression force provided by the user reduces the air gaps in the system, causing a rapid change in flux through the coil and results in an induced electromotive force and current flow through the coil. A spring and damper element is added to the system to counter the forces exerted by the magnets and the user. This returns the generator to some equilibrium position in preparation for another cycle. Additionally, this serves to convert mechanical energy stored in the springs during compression to electrical energy as the springs exert that force in returning the system to its steady state. A diagram of the electromechanical system design is shown in Figure 1.

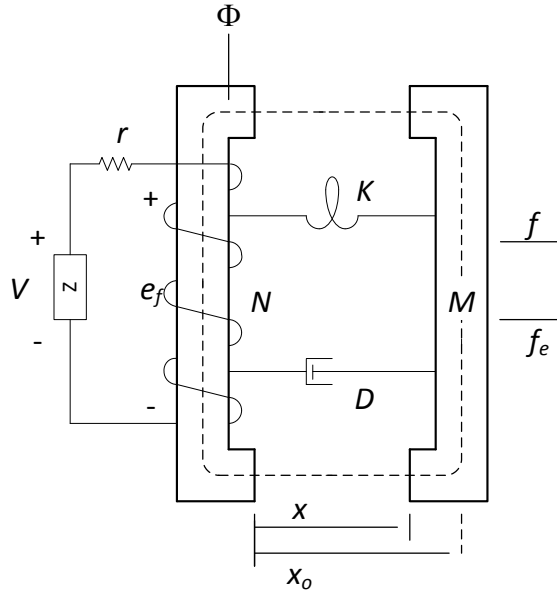


Figure 1. System Diagram of the Generator Electromechanical System Design.

Construction of the prototype incorporated simple inexpensive materials composed of ferrite cores, a wire coil, springs and permanent magnets. Behavior of the prototype was tested using different circuit component combinations connected to the coil leads. These combinations included a single capacitor, a half-wave rectifier and a voltage doubling circuit. All circuits utilized a combination of 470 μF capacitors and low forward voltage drop Schottky diodes when needed. The generator prototype is illustrated in Figure 2.

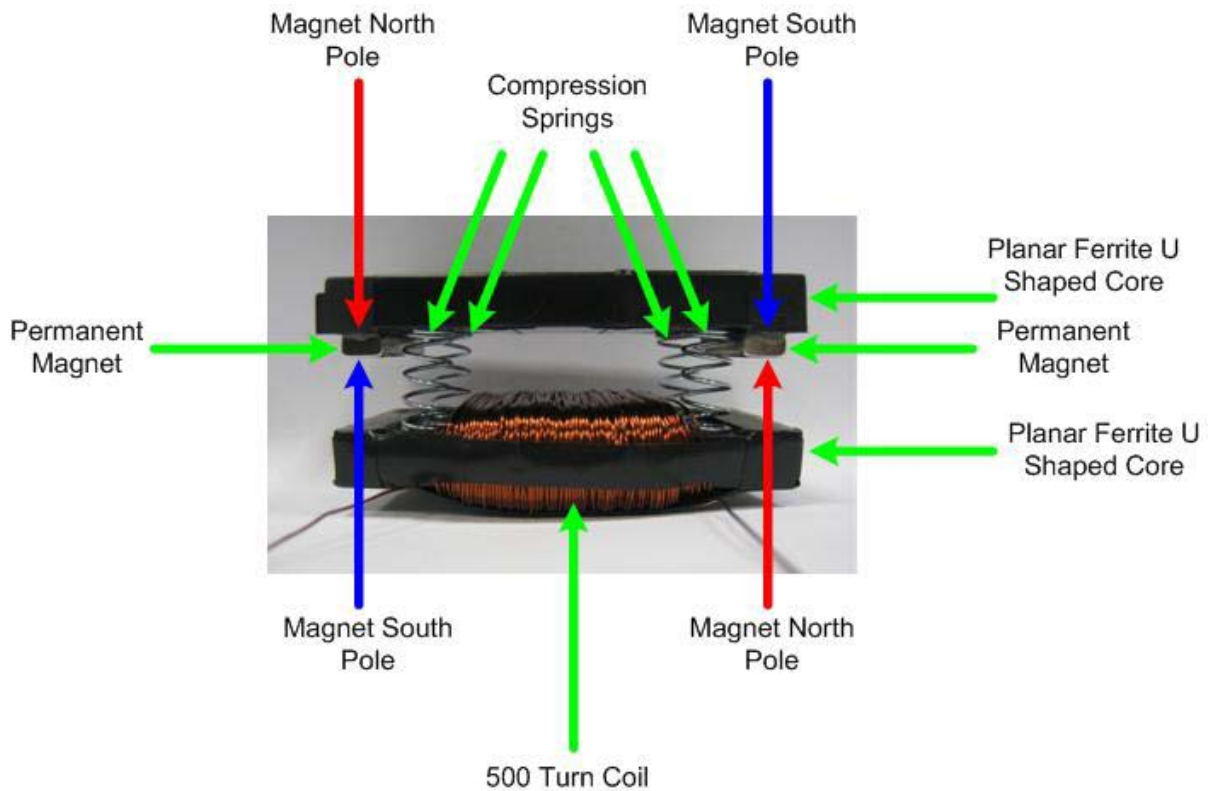


Figure 2. Constructed Generator Prototype.

Experimental testing investigated the generator's functionality with each circuit combination emphasizing the potential for the device to store the electrical energy in a method that could be utilized in electronic devices. Experimental data proved the functionality of the generator and its ability to store energy using both a half-wave rectifier and a doubling circuit. The doubling circuit proved to be the most effective by storing electrical energy generated during both the compression and release of the generator mechanism.

A computer simulation model of the generator system was developed in parallel with the construction of the prototype with the intent of using it for future optimization or related systems. The simulation exhibited similar behavior as seen in experimental testing, but is not yet accurate enough to predict the voltage and current precisely.

In conclusion, a miniature electromechanical generator was designed and realized. Experimental testing proved it's functionality to induce an electric current in a coil and a corresponding electromotive force. The ability to store this as electrical energy in capacitors was validated through experimental measurements.

LIST OF ACRONYMS AND ABBREVIATIONS

A	Amperes
AC	Alternating Current
cm	centimeters
DoD	Department of Defense
EM	Electromechanical
EMF	Electromotive Force
Hz	Hertz
IC	Integrated Circuit
MEMS	Microelectromechanical Systems
mH	millihenries
mJ	milliJoules
mm	millimeter
MMF	Magnetomotive Force
N	Newtons
Ω	ohms
μ F	microfarad
μ W	microwatts
rpm	revolutions per minute
V	Volts
W	Watts

THIS PAGE INTENTIONALLY LEFT BLANK

ACKNOWLEDGMENTS

I would first like to thank my thesis advisors, Professors Alex Julian and Giovanna Oriti, for their guidance and support through the completion of this thesis. Thank you for allowing me the creative freedom to pursue the possibilities in energy conversion. Without your patient direction and positive encouragement, this would not have been possible.

Most importantly, I would like to thank my beautiful wife, Donna, and my two engineers in training, Gabriela and Keira. Your unconditional love and support for all that I do mean the world to me. Thank you to my parents, brothers and sister for teaching me to work hard and persevere.

THIS PAGE INTENTIONALLY LEFT BLANK

I. INTRODUCTION

A. PURPOSE

The purpose of this thesis was to design and realize a completely autonomous system capable of converting mechanical energy provided by human motion to electrical energy. An increase in industry emphasis on low power engineering solutions involving microelectromechanical systems (MEMS) and integrated circuits (IC) has opened up the possibility to power such devices with such low power generators. As future devices continue to decrease in size and power requirements, a portable power generation device has the capability of becoming a viable alternative to batteries and a solution as a renewable energy source. The research done in this thesis aims at developing an inexpensive initial generator design and demonstrating its performance capability through experimental testing of a prototype.

B. MOTIVATION

Federal agencies have been directed by laws and an executive order to increase their use of renewable energy sources. The Energy Policy Act of 2005 requires that 7.5 percent of electrical energy used by federal agencies come from renewable energy sources by the year 2013. By fiscal year 2025, the goal is to increase that percentage to 25 percent total facility energy consumption [1].

The focus toward shifting to renewable and more efficient energy sources has become widespread in the Department of Defense (DoD), and specifically in the Department of the Navy. Specific goals were stated in April 2010, by the Secretary of the Navy Ray Mabus, calling for increased awareness in energy reform and conservation. Secretary Mabus ambitiously committed to have 50 percent of total energy consumption come from alternative sources by the year 2020. By the year 2016, the Navy is set to sail a “Great Green Fleet” composed of a carrier strike group made up of nuclear and hybrid ships, with aircraft and ships also running on biofuels [2].

Between the years 2000 and 2008, nearly \$600 million DoD dollars was spent on battery procurement. Of this, \$356 million was spent on nonrechargeable batteries and \$225 million on rechargeable batteries. That equates to about 61 percent of purchases going toward nonrechargeable finite energy source batteries. While electrical energy storage makes up a small percentage of defense costs compared to fuel, it still has cost-saving value and benefits to the service members who rely on its use daily [3].

Harnessing alternative energy sources for use is the key to meeting energy consumption goals of the future. To meet these goals, alternative energy solutions with DoD applicability need to be researched and developed immediately. Although the research in this thesis is unlikely to find a final solution to solve the DoD's energy needs or replace batteries altogether, it may provoke a plausible alternative energy solution.

C. BACKGROUND INFORMATION

The interest in energy harvesting from renewable energy sources has encouraged the investigation of miniaturized magnetically based power generation systems. Research has shown that electrically excited magnetic machines are not ideal for miniaturization due to scaling of the currents needed to produce magnetic fields in the systems. In contrast, permanent magnet systems have proven more effective in miniaturization since magnetic flux density is independent of the size of the magnet.

Most miniaturized generator designs fall into three broad categories: rotational, oscillatory and hybrid. Rotational generators are designed for continuous rotational operation at high speeds, allowing them to achieve a high power density. Oscillatory generators are usually designed to operate at some optimum resonance frequency. They generally employ a mass-spring-damper system utilizing small displacements between a magnet and coil [4]. Hybrid generators combine both topologies by utilizing an eccentric rotor to convert linear motion into rotational motion for power generation. The hybrid topology is

better suited to take advantage of a dynamic vibration frequency spectrum that may not be ideal for the oscillatory design [4]. The three general topologies are shown in Figure 1.

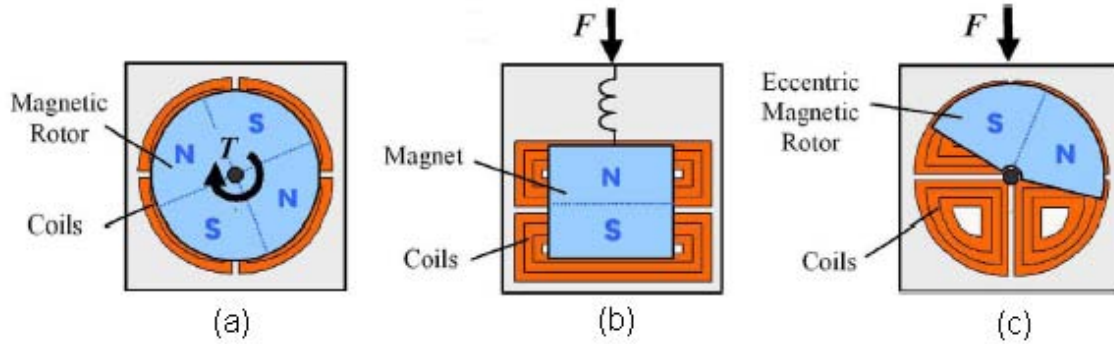


Figure 1. Three Miniaturized Generator Design Topologies: (a) Rotational, (b) Oscillatory, and (c) Hybrid. From [4]

Rotational generators operate using the same principles as their macroscale motor and generator counterparts. As a consequence of their reduced size, they tend to operate at higher rotational speeds and higher frequencies. Accompanying this higher operational speed is the ability to perform comparably to or better than large-scale generators of similar topology [4]. In 2002, a group from the Katholieke Universiteit Leuven in Belgium developed a single-stage axial microturbine that produced 16 W of power at a rotational speed of 100,000 rpm. This device had a housing diameter of 15 mm and a length of 25 mm while occupying a volume of only 5.63 cm³ [4], [6]. A joint effort by MIT and Georgia Tech in 2006 realized an axial-flux permanent magnet rotational generator of a much smaller size producing a maximum power of 8 W at 305,000 rpm. Around the same period, a French group from the Laboratoire d'Electrotechnique de Grenoble produced a similar result in an even more compact design using electroplated planar coils producing up to 5 W at 380,000 rpm. In contrast to the first microturbine design, the latter generators occupied a volume of less than 0.15 cm³ [4], [7]. More recent designs, such as that created by a team at Imperial College, demonstrated use of another axial-flux generator combined with an axial flux turbine to extract power from an externally generated

gas flow such as moving air [5]. These devices demonstrate the great power density potential of rotational designs, but also highlight the need for a prime mover source to provide for such high rotational operating speeds [4].

Oscillatory generator designs usually are designed to operate at some resonant frequency that matches the excitation vibration of the application. In turn, the mechanical system is also designed to this specification. These devices generally employ a mass-spring-damper system and, as a result, operate at frequencies much lower than rotational devices. They have demonstrated the ability to be more efficient in the use of substantial low-frequency excitation such as that utilized in portable or wearable electronics [5]. In the late 1990s, a team from MIT developed an oscillatory type generator system utilizing modeled vibrations from the walking motion of a person. The result was a 2-Hz operating frequency set to mimic the vibration of a device in a person's pocket. With a vibration amplitude of 2 cm, the generator produced a maximum output of approximately 400 μ W. Its functionality was demonstrated on a low power digital signal processing load [8]. A similar device worn at the belt was created by a team at Yamaguchi University in Japan. Their device produced a steady 3 V and 18.7 mW of power by incorporating a voltage-doubling circuit [4]. More recently, a pair from Switzerland developed a different approach using an air-cored solenoid linear generator design with a flexible hinge spring mechanism. When mounted below the knee, energy from the walking motion could be harvested with a mean output power of 35 μ W. Some universal commercial designs that operate at more natural occurring frequencies have been designed by companies such as Ferro Solutions and U.K-based Perpetuum [4]. The Ferro Solutions company has worked with the U.S. Navy in energy harvesting and offers a product that operates at a vibration frequency of 60 Hz and is capable of producing 5.2 mW from a generator volume of 170 cm³ [9].

Hybrid designs have been an attractive topology for operation in broader frequency spectrums. This design rotates an eccentric rotor when under forced linear acceleration of its pivot point. These designs have served well in

applications powering wrist watches. In 1988, the Seiko Company of Japan introduced the Automatic Generating System (AGS), utilizing an eccentric rotor design to power its wrist watches. A Swiss company, called ETA, developed a similar concept in its Autoquartz design. They utilized vibrations experienced by a watch to wind and release a spring that drives a gear powering a small generator. Both of these designs operate in the low μW range but prove very effective for their specific applications [4].

These generator designs prove the value and feasibility of small-scale and microscale magnetic power generator systems for use in portable electronics. Each design topology has certain characteristics making them better suited for specific applications. Rotational generators require a prime mover source to achieve high rotational speed requirements. Oscillatory designs tend to operate at resonant frequencies while hybrid designs have a broader frequency spectrum. Regardless of the differences, these generator designs have already proven capable to power wireless and embedded sensors, communication subsystems, implanted medical devices and other portable devices [4], [9]. Continued advancement in low power electronics and the increased power output of generator designs will inevitably result in the growing use of miniaturized generator designs as alternative energy sources.

D. APPROACH

The approach for completing this thesis was based on analysis of an electromechanical system followed by experimental testing of a constructed prototype. First, a basic linear electromechanical (EM) system that transfers electrical energy to mechanical energy, and the theory behind this conversion, was reviewed. This process was then reversed to try and turn mechanical energy into electrical energy. Secondly, magnetic circuit theory involving the actions of electromagnets to generate flux in a magnetic circuit was studied and used to predict the behavior of permanent magnets. Components and circuit configurations were researched for rectification and storage of the energy

harnessed from the generator. Several prototypes were constructed with different materials and different configurations to verify elements of the theory involved until a final design solution was concluded. Computer simulation models of the prototypes were created in parallel with the prototypes as a supplementary aid in future design optimization. This thesis focuses specifically on the presentation of the final design solution.

E. THESIS ORGANIZATION

The theory behind electromagnetic induction and the generator as an EM system design are presented in Chapter II. This design is explained in relation to the theory involving a general two-input EM system and the forces involved in a second-order spring and damper mechanical system. Components to construct the device are selected and their contribution to the system is explained in relation to the EM system theory.

The actual construction of the prototype, as well as the testing of the device, are detailed in Chapter III. Test setup and results are presented and performance is explained in detail.

A computer simulation model constructed in SIMULINK is explained in Chapter IV, and results of the simulated model are compared to experimental measurements obtained in Chapter III.

The results of the testing and conclusions about the generator performance are addressed in Chapter V, recommendations on future work are suggested for additional research regarding generator design.

II. DESIGN

A. INTRODUCTION

The theory of operation of the miniature generator, the steps taken for design of the generator, and selection of components for prototype construction are discussed in this chapter. The theory of operation will delineate the major parts of the generator, their interaction with other components and contribution to energy generation

B. THEORY OF OPERATION

1. Overview

The miniature generator design is an initial step in solving the energy demands of low power electronics in a manner that utilizes energy harvesting of human motion in a compact design. The concept employs Faraday's Law of Induction and basic, readily available components to transfer mechanical energy provided by the user to stored electrical energy. Design of the generator relies on principles of electromechanical systems and magnetic circuits.

2. Faraday's Law

Michael Faraday observed how current in a wire could produce a magnetic field, and hypothesized that the inverse could also be accomplished. He conducted experiments to prove that a magnetic field B could produce a current in a wire. After many failed experiments, Faraday eventually found success and discovered the key to what was termed "induction." Faraday found that "Magnetic fields could produce an electric current in a closed loop, only if the magnetic flux linking the surface area of the loop changes with time" [10]. Through his experiments, he found that current was induced in a loop whenever the magnetic flux in his system changed. He also found that the direction of the current induced in the loop was related to whether the flux was increasing or decreasing. If $B(t)$ represents a time varying magnetic field with some flux

linking the surface area of the loop S then a representation of a loop similar to the one Faraday used is shown in Figure 2. If a current I , such as the one in Figure 2, is induced in the loop, then a resulting voltage will be seen across the terminals 1 and 2. This process of generating this voltage is called electromagnetic induction, and the voltage itself is referred to as an electromotive force, V_{emf} .

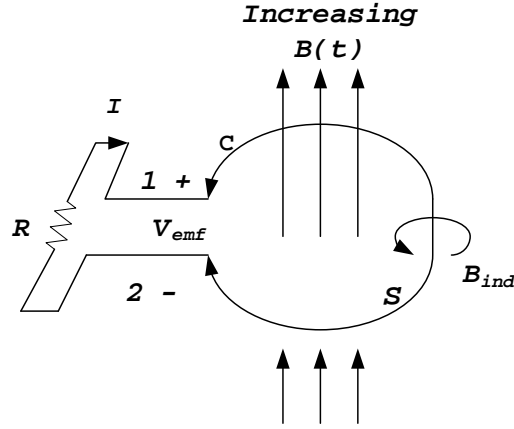


Figure 2. Stationary Wire Loop in a Changing Magnetic Field. From [10].

The V_{emf} induced in a coil of N turns is

$$V_{emf} = -N \frac{d\Phi}{dt} = -N \frac{d}{dt} \int_S \mathbf{B} \cdot d\mathbf{S} . \quad (2.1)$$

The current in the loop and the polarity of the electromotive force (EMF) in Figure 2 follow the principle of Lenz's Law. This law states that "The current in the loop is always in such a direction as to oppose the change in magnetic flux $\Phi(t)$ that produced it" [10].

The experiments of Faraday and the principles of electromagnetic induction are the basic building blocks for designing the miniature generator. Similar to the way Faraday experimented, the generator will contain a stationary loop linked by a time varying magnetic field to create an electromotive force. To accomplish this, the generator will be designed in an electromechanical system utilizing these components.

3. Electromechanical System

The miniature generator utilizes a linear electromechanical system where a single mechanical system interacts with a single electrical system through a common electromagnetic coupling field. As a result of this interaction between both systems, energy can be transferred from the mechanical system to the electrical system. This transfer of energy is illustrated in the block diagram shown in Figure 3.

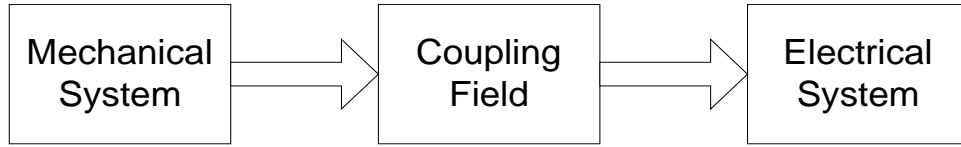


Figure 3. Block Diagram of Electromechanical System. After [11]

The transfer of energy from the mechanical system to the electrical system is not ideal, and losses will occur in each component of the system. Losses in the mechanical system occur due to heat from friction. Losses in the coupling field occur due to Eddy currents and hysteresis losses present in the ferromagnetic material. In this case, these losses have been associated with the electrical system instead of the coupling field resulting in the coupling field being considered a lossless field. Since the field will be independent of any small losses they can be neglected in design and analysis of the electromechanical system. If W_m is the mechanical energy transferred to the coupling field, W_{mL} is energy losses in the mechanical system and W_{ms} is the energy stored in the mechanical system, then the total energy supplied by the mechanical source W_M is

$$W_M = W_m + W_{mL} + W_{ms} . \quad (2.2)$$

Neglecting any losses in the coupling field, we find the total energy transferred and stored in the coupling field W_f . Losses in the electrical system account for nearly all of the losses in the realized system. These losses W_{eL}

occur from heat loss dissipation due to the resistance of the large coil used in the generator design. If W_e is the energy transferred to the electrical system from the coupling field, W_{es} is the stored electrical energy and W_{eL} are the losses in the electrical system, then the total energy generated is

$$W_E = W_{es} + W_{eL} + W_e . \quad (2.3)$$

Considering the law of conservation of energy and neglecting any field losses, we can write the transfer of energy as

$$W_f = W_e + W_m , \quad (2.4)$$

or

$$W_f = (W_E - W_{eL} - W_{es}) + (W_M - W_{mL} - W_{mS}) . \quad (2.5)$$

The coupling field for the system is considered conservative since no field losses are being considered. The balanced transfer of energy in the system is depicted in Figure 4.

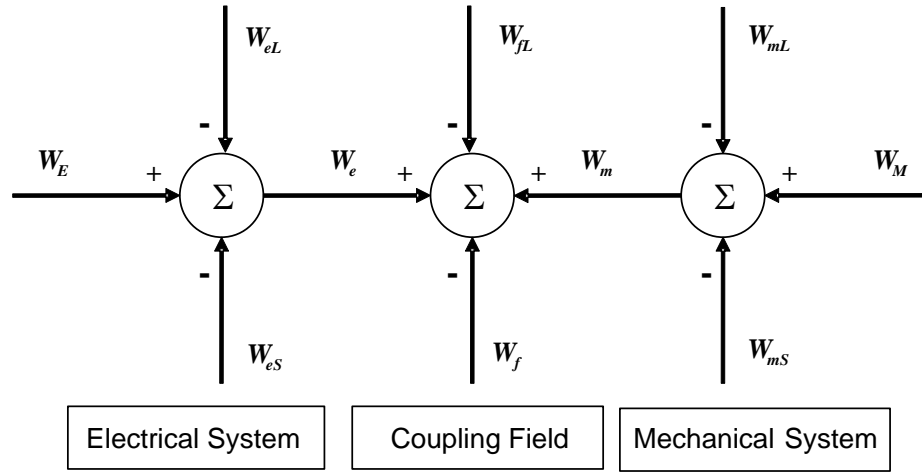


Figure 4. Energy Balance of Generator System. From [11]

The generator design is intended to be a realization of an elementary electromechanical system. As shown in Figures 3 and 4, the coupling field is the essential catalyst used for energy transfer in the generator system. For this generator design, a magnetic coupling field has been chosen as the means of energy transfer. The EM system diagram is shown in Figure 5. The external

mechanical force applied to the system by the user is denoted by f and the electromagnetic force that is present is f_e . The resistance associated with the coupling coil is r and the number of turns that make up the coupling coil is N with e_f being the voltage induced by the coupling field. The mechanical system includes K , the spring constant and D , the damping coefficient with M being the mass of the movable portion of the system. To represent the displacement of the system, x_o is the equilibrium position where the spring force is and x denotes the current position of the mechanical system. The flux in the magnetic circuit is represented by Φ . Given that there is only a single coupling field in the circuit, and assuming perfect coupling with negligible leakage, Φ represents the total flux in the magnetic circuit. Notice that x is defined to have positive displacement in the direction to the right.

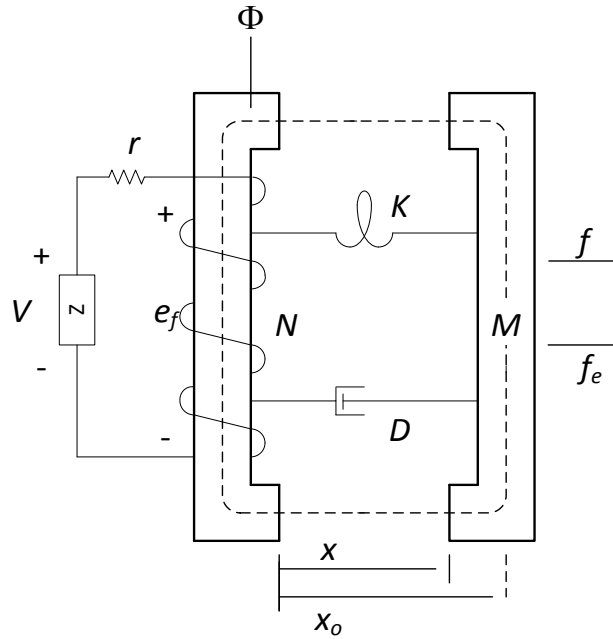


Figure 5. Electromechanical System Diagram. After [11]

The voltage generated across the storage element is represented by V and the Equation that describes this voltage is

$$v = ri + e_f, \quad (2.6)$$

where the voltage drop across the coupling field is

$$e_f = \frac{d\lambda}{dt} = \frac{d}{dt}(L(x)i(t)) = L(x)\frac{di}{dt} + i\frac{dL(x)}{dx}\frac{dx}{dt}. \quad (2.7)$$

Equation (2.6) can be written as

$$v = ri + L(x)\frac{di}{dt} + i\frac{dL(x)}{dx}\frac{dx}{dt}. \quad (2.8)$$

The total energy supplied to the electrical system is

$$W_E = \int vi \, dt. \quad (2.9)$$

Incorporating Equations (2.3), (2.6) and (2.9) together, we get the total energy supplied to the electrical system as

$$W_E = W_{eL} + W_e = r \int i \, di + \int e_f i \, dt. \quad (2.10)$$

Here W_{es} is zero since there are no energy storage elements on the electrical side. The total energy transferred to the coupling field specifically from the electrical system is

$$W_e = \int e_f i \, dt. \quad (2.11)$$

From Equation (2.8), it is shown that the voltage drop across the coupling field e_f is highly dependent on the change in inductance of the generator with respect to position and the change in position with respect to time (dx/dt). These two aspects of the operation of the generator are critical in regard to predicting performance of the generator and relating it to the inductance range of operation for the coil. Realization of the device must attempt to maximize the inductance range of operation for the generator from its equilibrium position to its closed position and the speed at which the position of the device can be changed.

The mechanical system behavior can be characterized by Newton's law of motion and incorporated in a 2nd order spring and damper system. Referring to Figure 5, we find the force equation for this system as

$$f = M \frac{d^2x}{dt^2} + D \frac{dx}{dt} + K (x_o - x) - f_e. \quad (2.12)$$

The total energy supplied by the user into the mechanical system is:

$$W_M = \int f \, dx = \int f \frac{dx}{dt} dt. \quad (2.13)$$

Incorporating Equations (2.2), (2.12) and (2.13) together, we obtain the total energy supplied to the mechanical system as

$$W_M = W_m + W_{mL} + W_{ms} = M \int \frac{d^2x}{dt^2} dx + D \int \frac{dx}{dt} dx + K \int (x - x_o) dx - \int f_e \, dx. \quad (2.14)$$

In Equation (2.14), W_{mS} is represented by the energy stored in the mass and spring while the damping coefficient D contributes to W_{mL} , losses due to heat and friction. The total energy from the mechanical system specifically transferred to the coupling field is

$$W_m = - \int f_e \, dx. \quad (2.15)$$

The electromechanical force represented in Equation (2.15) assumes that a positive force is in the same direction as the negative displacement of the system shown in Figure 5. Substituting Equations (2.11) and (2.15) into (2.4), we find the energy stored in the coupling field as

$$W_f = W_m + W_e = \int e_f i \, dt - \int f_e \, dx. \quad (2.16)$$

The electromagnetic force f_e can be determined by taking the total derivative of the energy stored in the coupling field W_f . To calculate this, an expression for W_f that describes the system must first be determined. If x , displacement, and i , current, are used as state variables to describe the electromechanical system, then x will be used explicitly to define the behavior of the mechanical system upon the coupling field.

The field energy of a linear, singly excited system can be expressed as

$$W_f = W_f(i, x), \quad (2.17)$$

where

$$W_f(i, x) = \frac{1}{2} L(x) i^2. \quad (2.18)$$

The generator design can be expressed by taking the expression in Equation (2.18) and expanding its application to a two input system with inputs i_1 and i_2 . The general expression for a two input system is

$$W_f(i_1, i_2, x) = \frac{1}{2}L_{11}(x)i_1^2 + \frac{1}{2}L_{12}(x)i_1i_2 + \frac{1}{2}L_{21}(x)i_2i_1 + \frac{1}{2}L_{22}(x)i_2^2, \quad (2.19)$$

and

$$W_f(i_1, i_2, x) = \frac{1}{2}L_{11}(x)i_1^2 + L_{12}(x)i_1i_2 + \frac{1}{2}L_{22}(x)i_2^2. \quad (2.20)$$

Equation (2.19) can be related to the field energy in the generator design, but must be modified to correctly represent an electromechanical system that utilizes permanent magnets. In the case of Equation (2.19), the second input is generally represented by an additional coil that couples to the field. Permanent magnets, by contrast, can be analyzed as a flux source representing the second input to the system. The field energy contribution of the permanent magnets will be discussed in detail later in this chapter.

The designed generator encompasses a linear time-variant EM system where the λ - i plot will result in a straight-line relationship for any fixed value of x . As x changes, the slope of the line changes, making it time variant. In this type of system, the coenergy W_c will be equal to the field energy W_f which can be useful in determining f_e . The total derivative of the expression found in Equation (2.19) yields a result for f_e that can be solved by either evaluating W_c or W_f :

$$f_e(i_1, i_2, x) = \frac{\partial W_c(i_1, i_2, x)}{\partial x}, \quad (2.21)$$

or

$$f_e(\lambda_1, \lambda_2, x) = -\frac{\partial W_f(\lambda_1, \lambda_2, x)}{\partial x}. \quad (2.22)$$

From Equations (2.19), (2.21) and (2.22), the electromagnetic force f_e contributed in the system and the energy in the coupling field W_f are dependent on each other, with the field energy directly being a function of the flux in the

electromechanical system [11]. As a result f_e is also dependent on the change in flux in the system as the displacement in the system changes. Consequently, the permanent magnets will play a critical role in the system design, and theoretically, if they are used as a flux source, the largest change in the flux contributed to the system from the magnets would yield a higher f_e and W_f .

C. COMPONENT SELECTION

1. Overview

The realization of the theory previously mentioned in this chapter into a working prototype involves transition of the EM system shown in Figure 5. into a working system using actual components. This section discusses the choice of components used to construct the generator prototype and details their contribution to the system.

2. Ferrite Cores

The magnetic circuit shown in Figure 5 requires a path to guide Φ , the flux in the magnetic circuit. In a similar manner, as current must travel through a completed path in an electronic circuit, the flux must also travel through a completed path in a magnetic circuit. To accomplish this, a ferromagnetic material behaving as a flux conductor has been chosen to guide the flux through the magnetic circuit. Ferromagnetic materials naturally exhibit strong magnetic properties since their magnetic moments tend to align along the direction of an external magnetic field. Additionally, they also remain partially magnetized after the removal of the external magnetic field [10].

In order to miniaturize the generator and maximize the available coil area around the ferromagnetic material, a thin rectangular core was suitable for the application. As a result, the split planar ferrite core shown in Figure 6 was chosen as the ferromagnetic material in the magnetic circuit. These cores are generally used around a ribbon cable for EMI interference suppression [12].



Figure 6. Split Planar Ferrite Core. From [12].

The cores are comfortable in size and can easily fit in the palm of a person's hand for use. Since the cores are typically used on ribbon cables they are manufactured in two matching elongated U-shaped pieces that fit together with only enough space between them for the cable to occupy. They also are fitted with a plastic case, shown in Figure 7, which could be used for additional protection during use in the intended mechanical environment. Ferrite cores are generally brittle and can break easily if handled aggressively, making them unreliable in applications where they will endure an impact. In this application, the plastic case will provide vital protection and prevent core breakage during use of the generator. It will also keep pieces of the cores from breaking off as a result of the strong magnetic fields they will be subjected to.



Figure 7. Planar Ferrite Cores in Protective Case. From [13]

An additional advantage to these cores is that they are cheap and easy to obtain in suitable dimensions. The main disadvantage to these particular cores is that they have lower permeability than other, more expensive, core materials and have lower saturation ratings. The application of the cores in the EM system is shown in Figure 8.

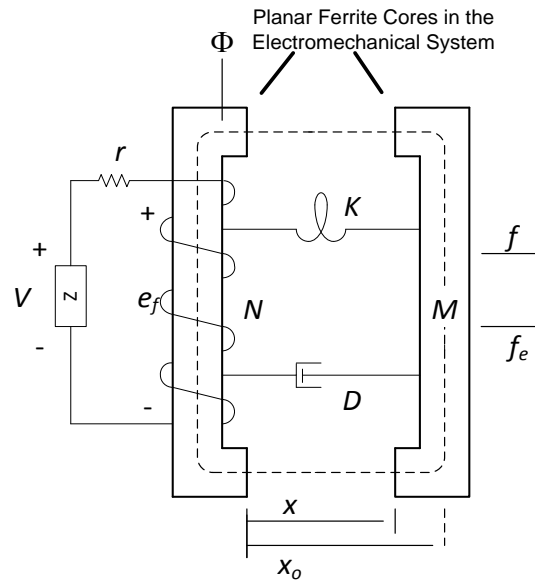


Figure 8. Ferrite Cores in the EM System Diagram. After [11]

3. Permanent Magnets

In order for the EM system to function as desired, it will require a magnetic field that can be controlled or regulated in some manner. From the previous section, we understand that the electromagnetic force f_e will play a crucial role in the energy being transferred to the coupling field, and is highly dependent on displacement of the system and a changing magnetic field. This magnetic field can be generated in two ways, either through the use of an electromagnet or a field created by permanent magnets. Either method will work to create the magnetic field; however, the use of a field created by an electromagnet will require an additional coil and voltage source to drive the electromagnet, and there will be losses due in the coil. Although this method would be great for

regulating the magnetic field, the system would be far from achieving the desired autonomy if it required a voltage source to function. To remedy this, and to make the system completely independent, permanent magnets are used instead.

To decide which type of permanent magnets will be used, the position of the magnets in the system will dictate how they will be required to function. To maximize the change in the magnetic field and its influence on the coupling field, the magnets have been positioned on the movable portion of the EM system on the raised ends of the ferrite cores. In this configuration, any change in the displacement of the system will cause a change in the magnetic field acting on the coil. In turn, this will limit the displacement of the system by the thickness of the magnets used but will also increase the area the coil can occupy. The position of the magnets in the electromechanical system is illustrated in Figure 9.

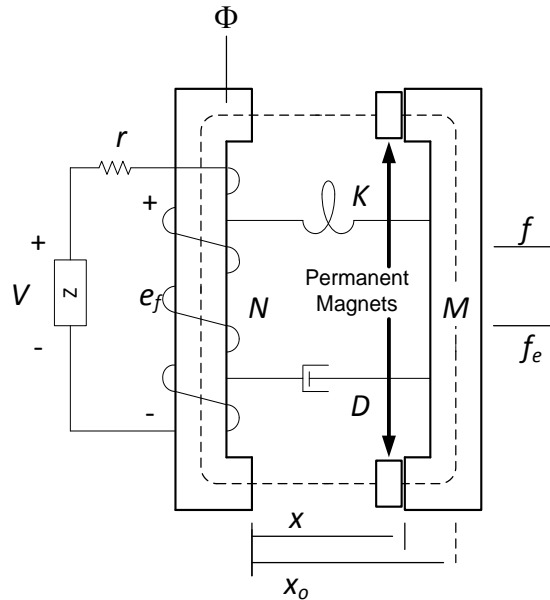


Figure 9. Permanent Magnet Position in the EM System Diagram. After [11]

Since the size and field strength of the magnets are critical limitations of the design, consideration for potential magnets seeks to maximize the field strength for the available area where the magnets can be positioned. As a result, neodymium magnets were specifically chosen to be used in the system. These

magnets are made of an alloy of neodymium iron and boron (Nd-Fe-B). They were specifically chosen because they offer the highest field strength of any magnets available. Additionally, a large assortment of these magnets is commercially available in different strengths, sizes and magnetization orientation for low costs [14].

Given the position of the magnets in the electromechanical system, a neodymium block magnet of similar dimensions as the extended portions of the U-shaped cores was chosen to maximize the flux contributed to the system. If the magnetic flux Φ is

$$\Phi = BA, \quad (2.23)$$

where B is equal to the magnetic flux density of the magnet, and A is equal to the cross-sectional area of the magnet, to maximize the flux in the system both of these variables should be made as large as possible [11]. The flux density is maximized by using a strong magnet, such as the neodymium magnet. The cross-sectional area of the magnet is maximized within the limitations of the design by matching it to the dimensions of the extended portions of the ferrite cores as closely as possible. By doing this, no area available for the coil or springs is compromised for the size of the magnet.

The position of the magnets also requires a specific magnetization direction to provide flux efficiently from one magnetic pole to the other. As mentioned in the previous section, the magnetic moments of the ferromagnetic material will align along the direction of the applied external magnetic field. If the flux path is to be guided through the EM system, as shown in Figure 9, then the flux must be issued from the permanent magnets into the ferrite cores from the face of the magnet toward the core. Given that flux is issued from the north pole of permanent magnets, the magnetization direction needed is illustrated in Figure 10.

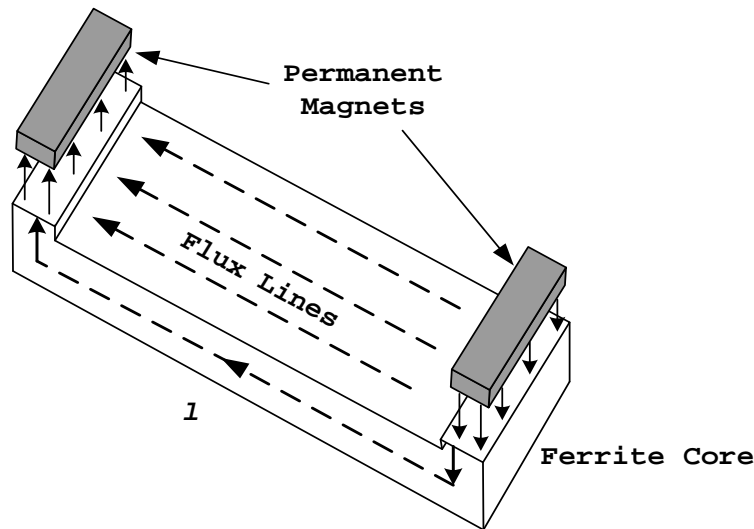


Figure 10. Flux Path Through Ferrite Core.

If the dimensions of the block magnet used are as shown in Figure 11, the magnetized direction should be through the thickness of the magnet. By aligning the north pole of one of the magnets toward the ferrite core and the south pole of the other magnet toward the same ferrite core, the largest amount of flux issued from the north pole of each magnet will couple to the system.

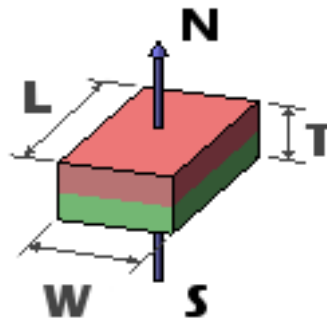


Figure 11. Magnetization Direction Through Thickness. From [15]

In order to meet the dimension requirements, magnetization direction and high magnetic field strength, a grade N42 Nd-Fe-B magnet one inch long, one-quarter inch wide and one-eighth inch thick was used in the generator design. This magnet is shown in Figure 12.

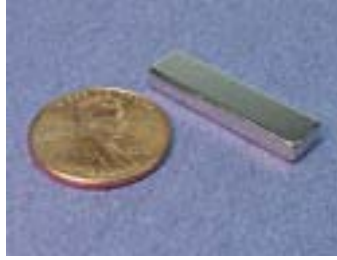


Figure 12. Grade N42 Nd-Fe-B Magnet Used in the Generator. From [16]

To further understand the behavior of the permanent magnets in the EM system, a circuit model of a magnet can be considered. Internally, the flux density of a magnet is not completely uniform with each part operating at a slightly different point. However, to simplify the magnet model, the assumption is made that it does have a uniform density. Additionally, the magnet is assumed ideal with a relative permeability equal to 1, or simply, the equivalent of free space. The magnet model shown in Figure 13 depicts the magnet as a flux source ϕ_r in parallel with the internal reluctance of the magnet R_m . If the magnet were in free space, the reluctance of the air gap between the magnet's poles is R_l . In relation to the EM system, R_l represents the reluctance of the air gaps associated with the displacement of the system. If ϕ_l is flux that passes through the load reluctance, then the demagnetizing flux ϕ_d represents the amount of flux that does not pass to the load. In the circuit model shown in Figure 13, this flux passes through R_m instead of R_l and can be considered as flux that couples back to the magnet itself instead of to the air gap.

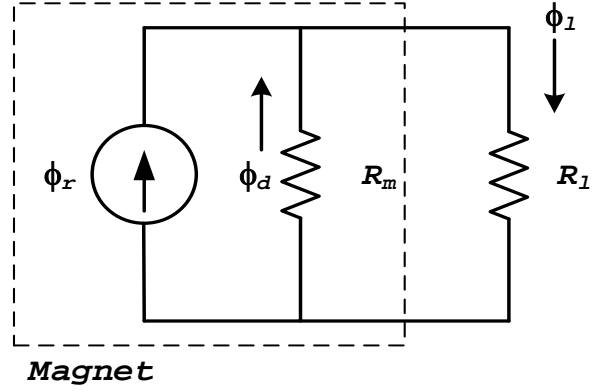


Figure 13. Circuit Model With Magnet Modeled as a Flux Source and Parallel Reluctance. From [17]

Flux in the circuit model is conserved with

$$\phi_r + \phi_d = \phi_l. \quad (2.24)$$

The magnetomotive force (MMF) loop equation for the flux path is

$$R_m \phi_d + c R_l \phi_l = 0. \quad (2.25)$$

Solving Equations (2.24) and (2.25) for the load flux, we get

$$\phi_l = \left(\frac{1}{1+c} \right) \phi_r. \quad (2.26)$$

In Equation (2.25), the variable c represents a scaling factor related to the permeance coefficient p_c used to determine the flux output of a magnet in various conditions. If the demagnetization factor of a magnetic circuit is

$$N_{magnet} = \frac{c}{1+c}, \quad (2.27)$$

then the permeance coefficient is related to N by

$$p_c = \frac{(1 - N_{magnet})}{N_{magnet}}. \quad (2.28)$$

Now the relationship of c to p_c is

$$p_c = \frac{1}{c}. \quad (2.29)$$

For a magnet in free space, c is dependent solely on the geometry and dimensions of the magnet used. When the magnet is placed in a circuit, c

depends not only on the magnet geometry but the circuit geometry as well [17], [18]. In a simple magnet circuit, such as Figure 13, it is more useful to determine c by normalizing the load reluctance to the reluctance of the magnet as given by

$$R_l = cR_m . \quad (2.30)$$

By normalizing c in this manner and applying it to the EM system, c relates directly to the ratio of the air gap of the system in comparison to the thickness of the magnet [17]. For this relationship ratio to be a valid assumption, the permeability of the ferrite cores must be high enough that the reluctance of the air gap dominates the reluctance of the magnetic material. The circuit can then be evaluated using a flux divider in the same way an electric circuit uses a voltage divider to solve for a voltage across a load. As the displacement in the system decreases, the air gap gets smaller, thus, making R_l smaller and more flux couples to the load. When the displacement is large, R_l is greater and less flux couples to the load. To illustrate this concept further, a magnet in free space with $R_l \gg R_m$ where $\phi_r = \phi_d$ and ϕ_l equal to zero is shown in Figure 14. In this theoretical example, R_l is very large, and all the flux issued from the magnet's north pole couples to the south pole.

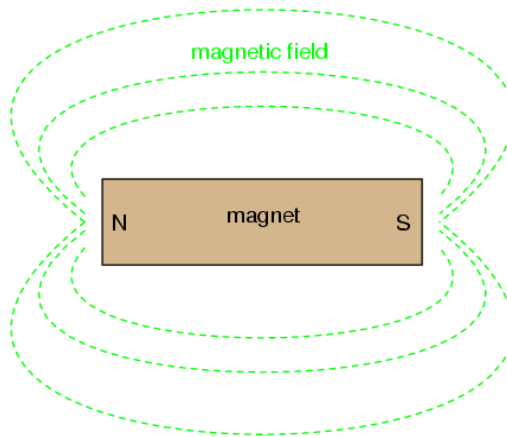


Figure 14. Permanent Block Magnet in Free Space. From [19]

A magnetic circuit illustrating the EM system, where x is the displacement of the system with an air gap occupying the area between the magnets and the

ferrite core, is shown in Figure 15. In both cases of this example, R_l has a direct relationship to the size of the air gap. In the example (a) of Figure 15, x and R_l are both large, resulting in less flux coupling to the system. In the example (b) of Figure 15, x and R_l are both small, resulting in more flux coupling to the system. In this case, c can be expressed as a function of x and the load flux and reluctance relationships in the system are

$$\phi_l = \left(\frac{1}{1 + c(x)} \right) \phi_r \quad (2.31)$$

and

$$R_l = c(x)R_m. \quad (2.32)$$

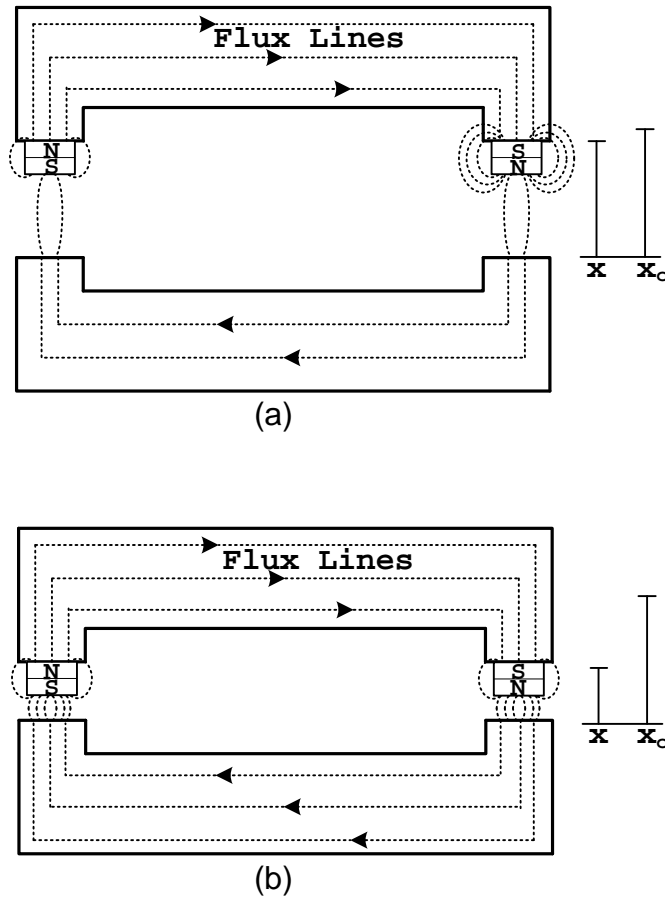


Figure 15. Magnetic Circuit Representation of EM System With (a) Large x and R_l and (b) Small x and R_l .

The normalized relationship of c can be further verified by considering the Thevenin magnet model equivalent of Figure 13 and its implementation in a magnetic circuit model for the EM system.

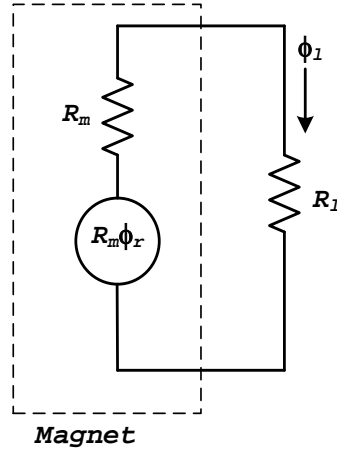


Figure 16. Thevenin Equivalent Circuit Model of a Magnet. From [17]

If the permeability of the core is assumed to be much greater than that of air, and the reluctance of the core is neglected, a simplified magnetic circuit model of the EM system can be made by expanding the Thevenin model (shown in Figure 16) wherein solving the circuit is analogous to an electrical circuit. The EM system magnetic circuit is shown in Figure 17. Solving this circuit for ϕ_1 , we confirm the use of (2.31) and the normalized use of c in Equation (2.32).

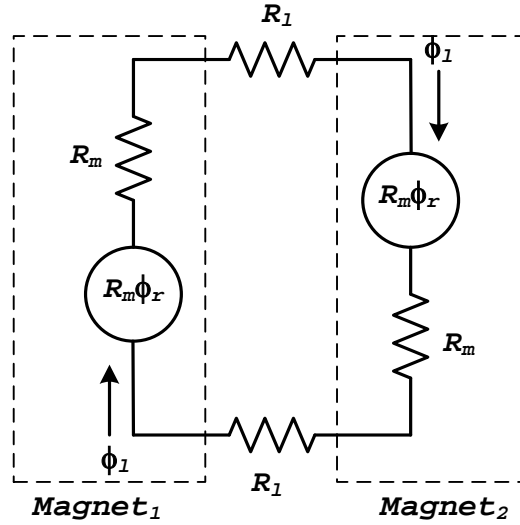


Figure 17. Equivalent Magnetic Circuit for EM System.

Energy stored in the magnetic field of the permanent magnets W_{mag} can be considered as the ability of the magnet to perform mechanical work. This stored energy in the magnet is delivered to the system as mechanical work when a ferromagnetic keeper is applied to the system that completes the magnetic circuit. If the magnet is perfectly shorted by the keeper material, then the stored energy in the magnet is all delivered to the system as mechanical work, and the stored energy will go to zero. In the system shown in Figure 9, the ferrite cores act as a keeper to the permanent magnets delivering the energy stored in the magnetic field of the permanent magnets to the system as mechanical work. To determine the energy stored in the magnetic field of the permanent magnets, an expression can be derived through the summation of the energy stored in each reluctance where

$$W_{mag} = \frac{1}{2} (R_m \phi_d^2 + c(x) R_m \phi_l^2) \quad (2.33)$$

and

$$W_{mag} = \frac{1}{2} \left(\frac{c(x)}{1+c(x)} \right) R_m \phi_r^2. \quad (2.34)$$

Recalling Equation (2.18), where the energy stored in the coupling field is a function of $L(x)$ and i^2 , we see that the energy stored in the magnetic field is also related to (2.18). If R is reluctance and N is equal to the number of turns of a coil, then

$$\phi = \frac{Ni}{R} \quad (2.35)$$

and

$$L = \frac{N^2}{R}. \quad (2.36)$$

Substituting Equations (2.35) and (2.36) into general forms of the field energy equations, we obtain

$$W_f = \frac{1}{2} Li^2 = \frac{1}{2} \frac{N^2 i^2}{R} \quad (2.37)$$

and

$$W_{mag} = \frac{1}{2} k_s R \phi^2 = \frac{1}{2} k_s R \left(\frac{Ni}{R} \right)^2 = \frac{1}{2} k_s \frac{N^2 i^2}{R}. \quad (2.38)$$

If k_s is a scalar constant, then Equations (2.37) and (2.38) demonstrate that the field energy in a coil and that of a magnet can be expressed together [11], [17]. The general equation for the total energy stored in the coupling field of a two input system utilizing two coils is shown in Equation (2.20). Since the EM system of the generator is a two-input system containing a coil and permanent magnets, the field energy contribution of the second coil must be converted to that of the permanent magnets. The expression for the total energy stored in the coupling field is

$$W_f = \frac{1}{2} L(x) i^2 + i \left(\frac{1}{1+c(x)} \right) \phi_r + \frac{1}{2} \left(\frac{c(x)}{1+c(x)} \right) R_m \phi_r^2. \quad (2.39)$$

4. Compression Springs

Compression springs play a role in the EM system by storing mechanical energy when they are compressed. When a user compresses the generator, thus decreasing the displacement of the system, mechanical energy is converted to electrical energy. Additionally, this force provided by the user compresses the

springs. Mechanical energy is stored in the spring and delivered to the system when the generator is released. Springs represented in the EM system are shown in Figure 18, where K is the spring constant and D is the damping coefficient. The spring constant and dimensions of the spring are very important because the springs in the system must be able to overcome the tendency of the magnetic field provided by the permanent magnets to reduce the displacement of the system. The spring free height in conjunction with the spring constant inherent in its manufacturing are used to counter the attractive force of the magnets and determine the equilibrium position of the system. To counter this attraction and stabilize the system, four springs are used and mounted close to the magnets in the system. Additionally, since the springs are the only mechanical structures separating the two ferrite cores, their free height determines the equilibrium position x_o of the system. The positioning of the springs in the generator is shown in Figure 18.

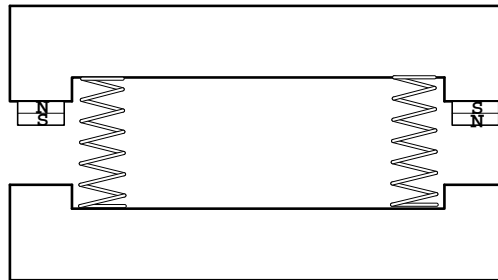


Figure 18. Generator With Springs Positioned Close to the Magnets.

The size of the springs must be carefully considered, since the area occupied by the springs reduces the available area for wrapping the coil.

5. Inductance Coil

An inductance coil is used as a means to store the magnetic energy in the EM system [10]. To construct the inductor, magnet wire was used and wrapped tightly around one of the ferrite cores. The coil area was limited to the space between the springs, and the height was limited by the area between the two

ferrite cores when the displacement of the system was at a minimum. This limitation on the coil area is shown in Figure 19.

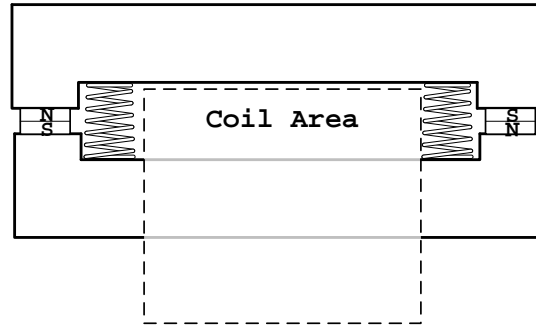


Figure 19. Compressed Generator With Coil Area Limitations

Since the MMF voltage of the inductor is the product of N , the number of turns in the coil, and i the current through the coil, maximizing the number of coil turns in the available area was very important [11]. Additionally, smaller wire used to make the inductor creates higher resistance and, consequently, higher losses due to heat in the electric circuit. For these reasons, magnet wire was chosen to construct the inductance coil instead of traditional rubber-insulated wire. Magnet wire uses a film insulation that is very thin, allowing it to have a larger cross-sectional area of copper than rubber-insulated wires of the same circumference. By reducing the size of the insulation, an equivalent number of turns could be strewn around the core while increasing the cross-sectional area, thus reducing the resistance of the coil. To construct the generator, 28-gauge magnet wire was wound tightly in successive layers for 500 turns in the coil area shown in Figure 19.

6. Electrical Energy Storage

The current induced in the inductor coil and subsequent MMF voltage created needs to be stored in some manner for use. The EM system shown in Figure 5 has some impedance element z in series with a resistor, where z represents an element or network of elements used for energy storage. If z were simply replaced by a capacitor used for energy storage, the single capacitor

theoretically would charge and discharge immediately during the compression and release of the generator. Following the principle of Lenz's law, mentioned earlier in this chapter, we see that the current will flow in the coil in a direction to oppose the change in flux. To remedy this, rectification of the flow of current is used so that discharge of one or multiple capacitors is limited.

The first method used is a half-wave rectifier using a single Schottky diode D_s in series with a capacitor C where R is the resistance associated with the inductor coil L . This circuit is shown in Figure 20.

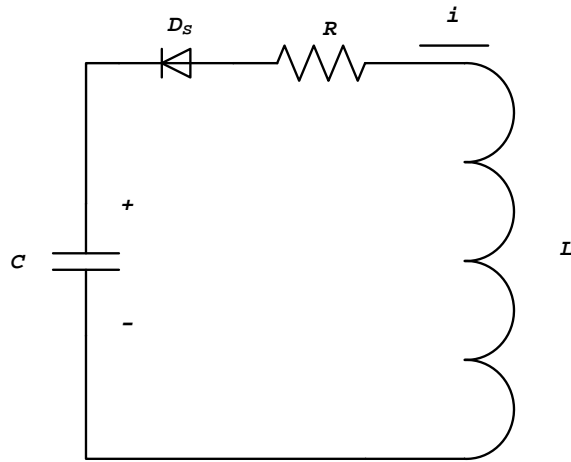


Figure 20. Half-Wave Rectifier Circuit

The half-wave rectifier takes advantage of the properties of the diode to restrict the flow of current in one direction only. By doing this, the capacitor will not discharge with a reverse in the change in flux during compression and release of the generator. Given a polarity-independent capacitor, the diode can simply be flipped to take advantage of either the change in flux during compression or release of the generator. This rectifier is limited because it only takes advantage of energy transferred during compression of the generator or release, but not both. Additionally, the voltage drop across the coil must be sufficient to overcome the inherent voltage drop associated with the diode or the capacitor will not charge. The voltage drop across the diode in the circuit has

been limited by using a Vishay™ 10BQ015 Schottky diode with a typical forward voltage drop of 0.35 V with 1 A of current [20].

The second method used for energy storage was a voltage-doubling circuit. This circuit uses a configuration that combines two half-wave rectification circuits together. It utilizes two capacitors and two diodes, and has the capability of storing the energy from both the compression and release of the generator. This circuit is shown in Figure 21.

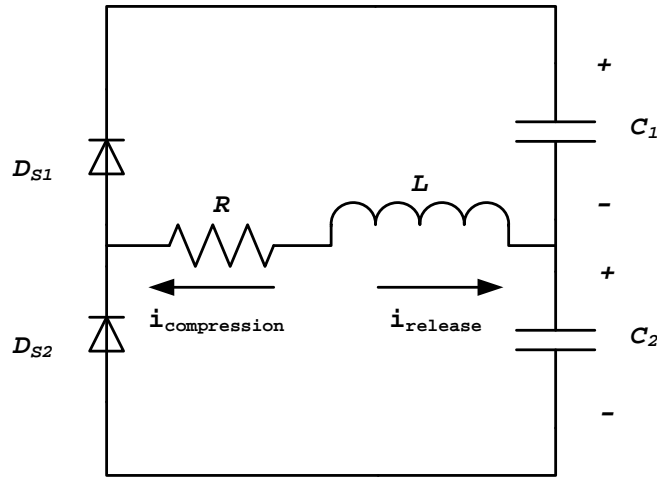


Figure 21. Voltage Doubling Circuit

Similar to the half-wave rectifier circuit, the doubling circuit needs to overcome the voltage drop associated with the diodes D_{S1} and D_{S2} but only has to account for the voltage drop of one diode during compression and release of the generator. The drawback of the circuit design is that two capacitors must be used for energy storage. However, it minimizes the voltage drop associated with adding additional diodes for rectification as in the case of a full-wave rectifier where each compression and release has to overcome the voltage drop of two diodes instead of only one.

D. CHAPTER SUMMARY

This chapter detailed the theory behind the operation of the generator to convert mechanical energy to electrical energy. It diagrammed the generator as an electromechanical system and detailed the conversion of energy in this system. Components were chosen to realize the generator, and the theory behind their role and contribution to the system was explained in detail. In the next chapter, construction and performance testing of a prototype of the electromechanical system will be examined.

III. PERFORMANCE TESTING OF PROTOTYPE

A. INTRODUCTION

An EM system was designed and components to realize the system were chosen. This chapter details how the components are combined to build a prototype of the EM system. Additionally, testing of the device ensues to demonstrate its performance.

B. PROTOTYPE CONSTRUCTION

The prototype miniature generator was constructed using the components detailed in the previous chapter and the steps provided in this section.

1. Core Preparation

Since the ferrite cores can break easily and also to shield the magnet wire from any sharp material, the cores were insulated with electrical tape in all exposed areas. This also ensured the integrity of the core material in the air gap when subjected to the strong magnetic fields of the magnet, preventing small powder pieces from breaking off and settling on the magnets. By insulating this area, the minimum displacement of the system is equal to the width of one layer of electrical tape insulation of 17 millimeters (mm).

2. Spring Placement

Once the ferrite cores were prepared with insulating material, the compression springs were ready for placement. To ensure stability of the device, four springs of equal dimensions were used and placed at the four corners of the inset portion of one U-shaped core. The springs are set as wide apart as possible to ensure maximum coil area is available for winding. The springs used in construction of the prototype had a diameter of 7.95 mm with a free height of 15.875 mm. They were attached to the ferrite cores using a strong adhesive.

3. Coil Winding

With the springs in position, the coil is ready for winding. To ensure there was no interference between the coil and springs during operation, small plastic walls were manufactured and placed in the boundaries between the coil area and springs. The coil was wound tightly in layers that run the length of the inset portion of the U-shaped cores. Nine layers accumulating 500 turns of the 28-gauge magnet wire encompass the coil in the generator prototype.

4. Core Alignment

The ferrite core realizing the movable member in the EM system must be attached next. This matching core should be lined up with the opposite ferrite core and attached to the springs using the same strong adhesive. At this point, the system is merely held together at the points where the springs and the ferrite cores meet.

5. Magnet Placement

The placement of the permanent magnets is the last step in construction and is also the most critical. The magnetization direction of the magnetic poles must be placed in the correct orientation for the generator to work properly. To ensure this correct orientation, the magnets were tested using a pole identifier. The magnets were placed on the ferrite core opposite the winding with one magnet north pole facing the core and the other magnet south pole facing the same core. Since flux is issued from the north pole and attracted to the south pole, this ensures that the flux is guided through the ferrite core without any repelling action. The magnets were set in place using a cold weld adhesive to prevent movement of the magnets during operation of the generator. The 3.175-mm thickness of the magnet, in addition to the minimum air gap, results in a minimum displacement of the system to be 3.345 mm. The resulting completed prototype is shown in Figure 22.

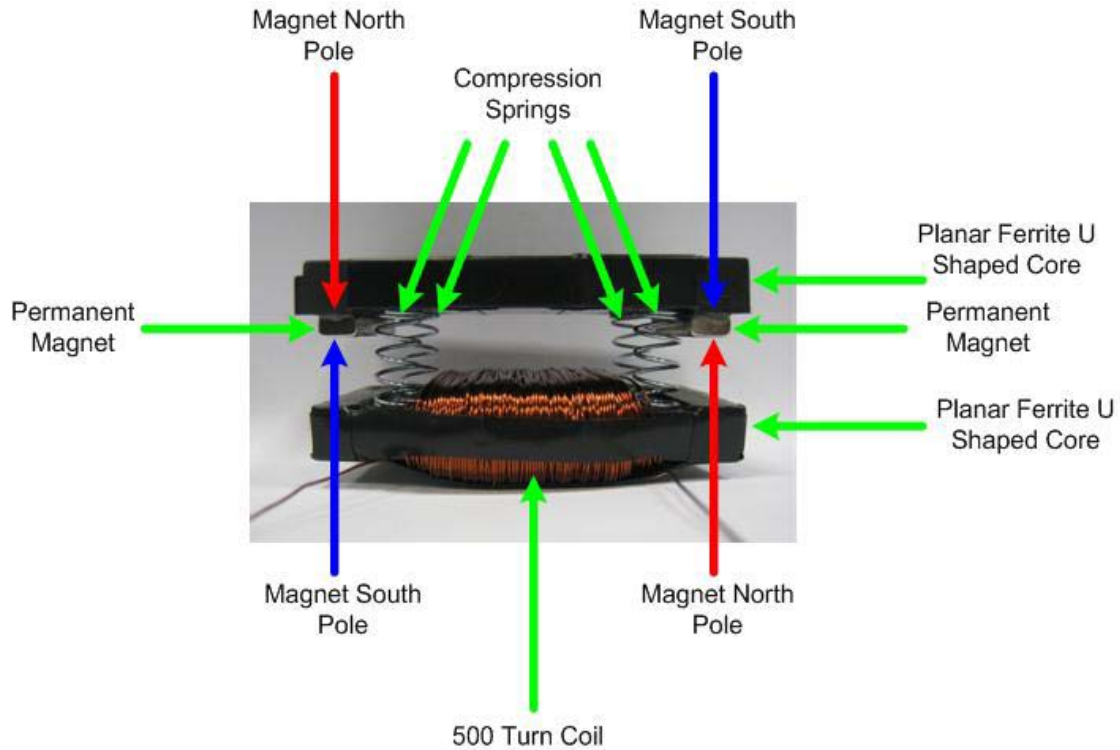


Figure 22. Miniature Generator Prototype.

C. TEST RESULTS

A range of tests was conducted on the generator to verify its operation and performance. The initial test inspected the experimental inductance range at which the generator operated. A LCR meter was used at different displacements of the system to measure the inductance of the coil at specific operating points, as shown in Figure 24.

The following tests measured performance of the generator with various energy storage circuits connected to the generator coil. Using a Tektronix™ oscilloscope, current probe amplifier, current probes and a voltage probe, measurements of both current and voltage data were recorded. This data was manipulated using MATLAB™ software to generate data plots of the voltage, current, power and energy in the tested circuit configurations. A general test equipment setup is shown in Figure 23.

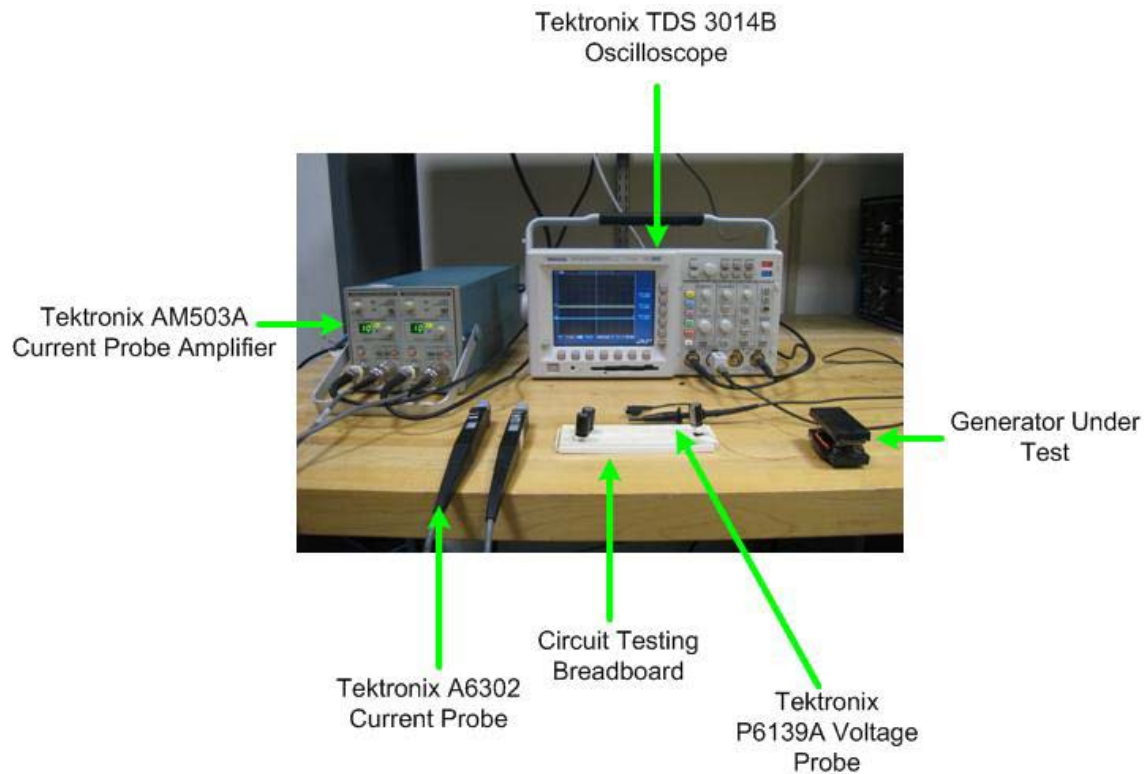


Figure 23. General Test Equipment Setup

1. Inductance Operating Range

In the previous chapter, it was mentioned that the EMF induced from the generator was related to a time-changing magnetic flux. If the inductance of the coil in the generator is also directly related to the flux in the magnetic circuit, this change in flux in the circuit also reflects a change in the inductance measurement of the coil. As a result, the largest change in the inductance with respect to the change in displacement of the EM system should produce a higher EMF.

To map the inductance of the coil in relation to the displacement of the EM system, the generator was tested using a Quadtech™ 7600 LCR meter at different displacements ranging from completely compressed to the equilibrium position of the device. The LCR meter was set to measure inductance in the coil using a one volt (V) peak-to-peak alternating current (AC) signal at 10 Hertz (Hz)

for test. An equal number of sheets of paper were placed in the air gaps to change the displacement of the system and were measured using a digital micrometer. Two sheets of paper were added to increase the displacement between each trial until the generator returned to its equilibrium position. The resulting measurements are plotted in Figure 24.

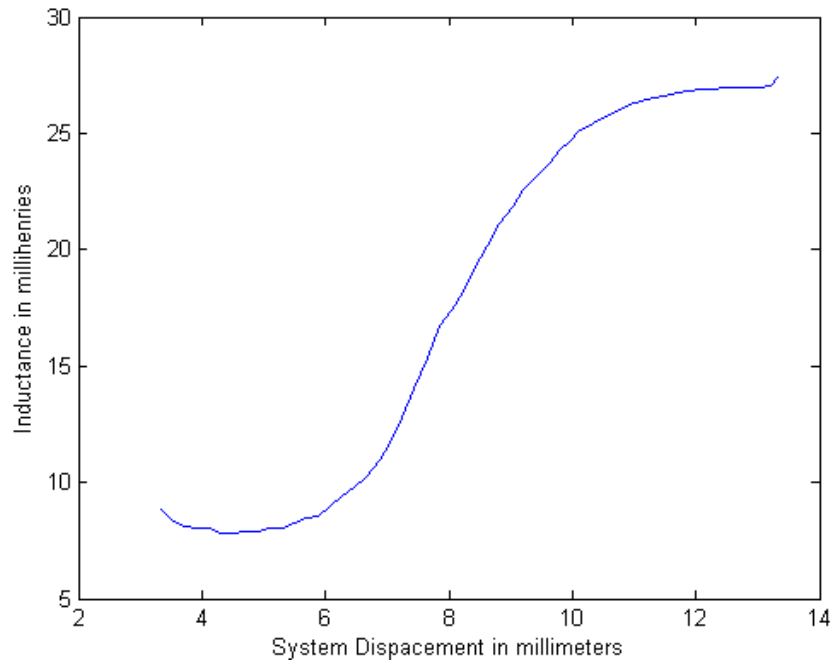


Figure 24. Inductance vs. Generator Displacement

From Figure 24, it is shown that the inductance of the generator coil decreases as the displacement of the system decreases. Using ferromagnetic materials with a high permeability usually causes the inductance of the coil to increase as the air gap is decreased. This phenomenon demonstrates that the ferrite core is operating in a specific area on its hysteresis curve known as saturation. In this area of the hysteresis curve, increases in the magnetizing force do not cause appreciable gains in the magnetic flux density of the material, causing the slope of the B-H curve to decrease until it becomes close to the magnetic constant μ_o [21]. This slope in the B-H curve is equal to the permeability of the material, which decreases rapidly when operating in

saturation. Permeability, in turn, affects the ability of the ferrite cores to conduct flux and is proportional to the inductance of a component [22], [23].

2. Single Capacitor Storage Element

The initial test to measure the functionality of the generator used a single 470 μF electrolytic capacitor in series with the leads of the coil. In this test, different aspects of a single stroke of the generator were analyzed using an oscilloscope. To define the different parts of a generator stroke, the compression stroke is considered displacement of the system from its open equilibrium position to minimum displacement. The release stroke consists of the generator starting in a closed position at minimum displacement and then being released to its open equilibrium position. A full stroke of the generator is considered to be the combination of the compression and release of the generator.

This test used a voltage probe measuring the potential between the leads of the capacitor and outputting this data to an oscilloscope. In addition, a current probe was placed on the coil lead connected to the positive capacitor lead to and data measurements sent to the same oscilloscope. The circuit test setup is shown in Figure 25. The resistance of the coil used in the generator measured to be 6.25 Ω and the capacitor was 460 μF .

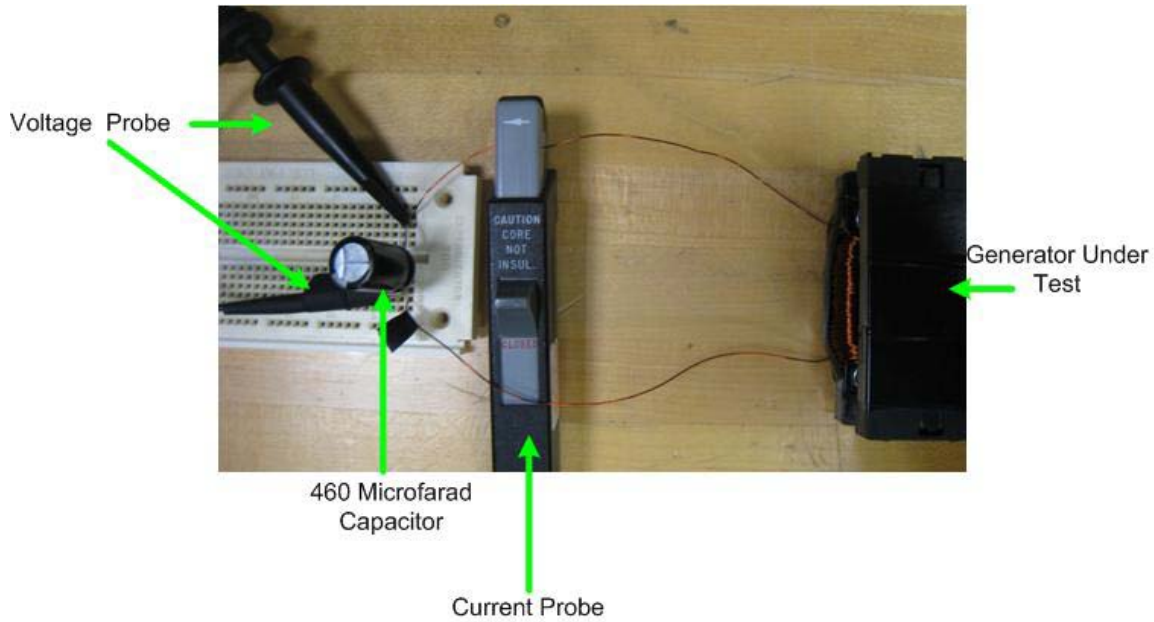


Figure 25. Single Capacitor Storage Test Circuit.

a. Full Stroke

To verify that the generator is generally functioning as expected, a full stroke test is done first. The expectation is to see two distinct events during compression and release that happen in succession. These events are characterized by apparent spikes in voltage and current that are proportional to changes in flux in the magnetic circuit. A plot showing the data collected for one test of a full stroke of the generator is shown in Figure 26.

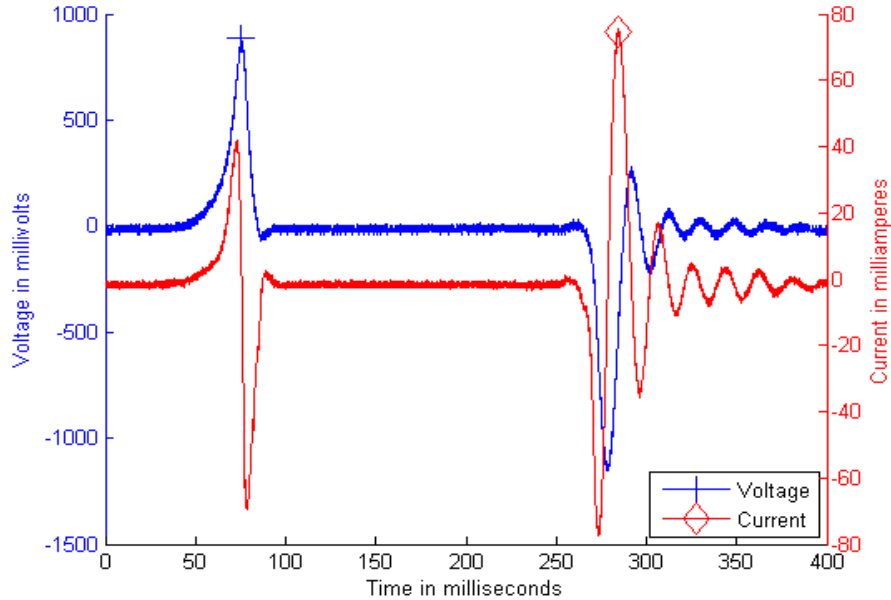


Figure 26. Full-Stroke Voltage and Current Generated Across Capacitor Terminals.

From the voltage and current data shown in Figure 26, two distinct events are clearly displayed delineating the compression and release of the device in order. The two events begin with voltage and current spikes in opposite directions typical of what is expected from the principle of Lenz's Law explained in the previous chapter. From inspection of Figure 26, the voltage and current does not ring during the compression stage since the system is at a minimum displacement where the cores and magnets are pressed together. In contrast, during the release stage, the voltage and current displays a ringing behavior due to the movement in the spring while it decompresses and oscillations occur in the system as it returns to an equilibrium position. Damping behavior is evident in the system as the magnitude of each oscillation decreases as the system returns to equilibrium. The power generated during the events is shown in Figure 27.

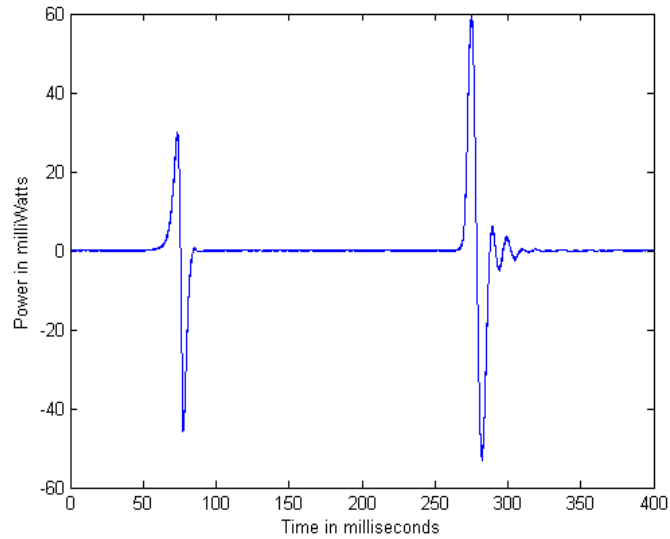


Figure 27. Full-Stroke Power Generated Across Capacitor Terminals.

The power data illustrates the product of the voltage and current generated during the two events. Comparing the peak power of the two events, we see that the power spike during the release is almost twice that of the compression. Integrating the power data with respect to time, we get the electrical energy seen by the capacitor shown in Figure 28.

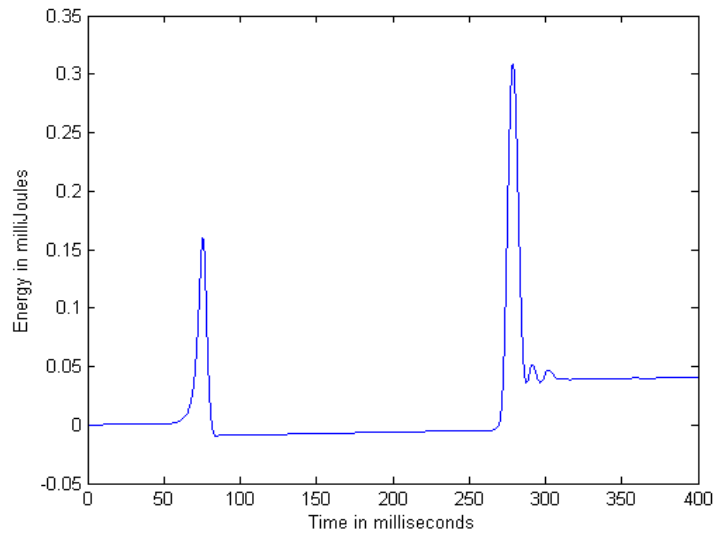


Figure 28. Full-Stroke Energy Generated Across Capacitor Terminals.

b. Compression Stage

Now that it has been shown that the generator is functioning through the full stroke spectrum, an additional test was conducted focusing on the compression stage only. This allows examination of this portion in a higher resolution compared to the entire full-stroke test. The voltage and current data collected is shown in Figure 29.

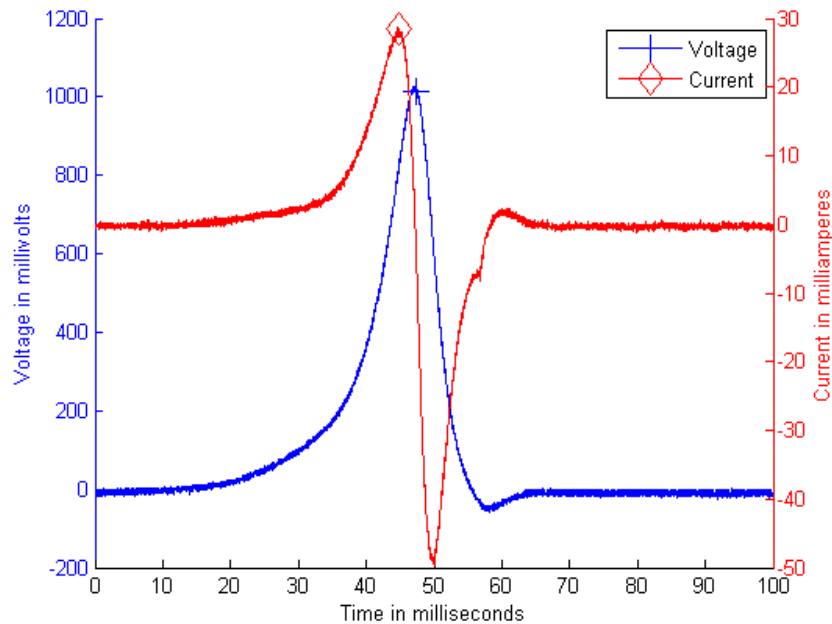


Figure 29. Compression Stage Voltage and Current Generated Across Capacitor Terminals.

From the voltage and current plot, the voltage across the capacitor increases while the current is positive, charging up the capacitor to a value of approximately one volt. When the current reverses direction and becomes negative, the voltage across the capacitor leads decreases as the capacitor voltage discharges. The product of the voltage and current data is shown in the power generated plot in Figure 30.

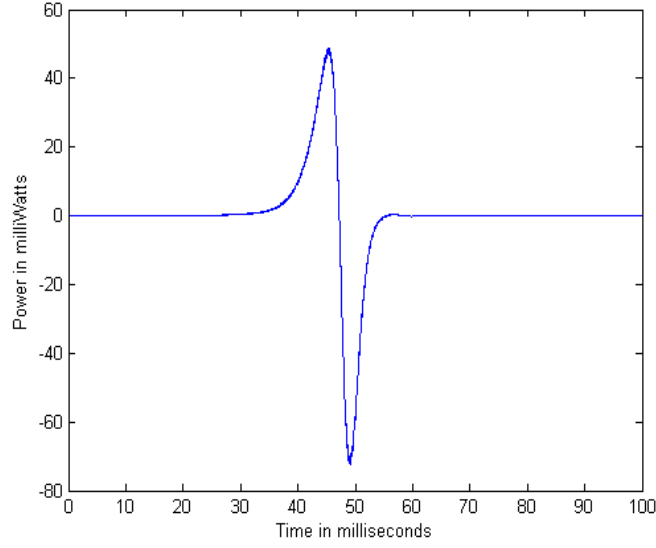


Figure 30. Compression Stage Power Generated Across Capacitor Terminals.

The power generated in the compression clearly shows power spikes in the positive and negative direction that mirror the polarity of the current in the coil. The resulting energy in the capacitor is shown in Figure 31.

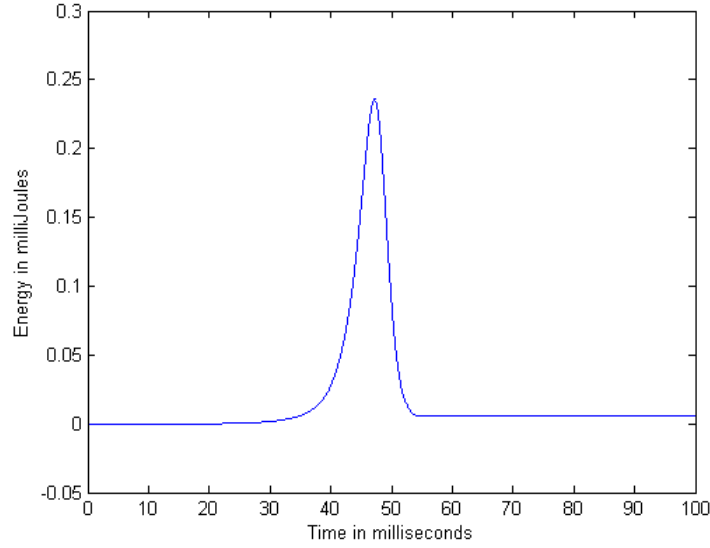


Figure 31. Compression Stage Energy Generated Across Capacitor Terminals.

The energy in a capacitor is equal to

$$E_{cap} = \frac{1}{2}CV^2. \quad (3.1)$$

The energy in the capacitor can be predicted by analyzing a point in the energy data plot [24]. If the voltage across the capacitor peaks at 1.024 V as shown in Figure 29, and the capacitor value is measured to be 459 μF , then the peak energy in the capacitor should correspond to approximately 0.24 mJ. This expected energy peak agrees with the energy values shown in Figure 31. Additionally, since the capacitor voltage is charging and then discharging with the change in polarity of the current, the net energy after these events theoretically should return to zero. This is confirmed by the spikes in power during charge and discharge of the capacitor and no net energy retained in the energy plot.

c. Release Stage

The current and voltage data during the release stage is shown in Figure 32. During the release, we expect the initial change in magnetic flux in the magnetic circuit to be opposite in direction as the compression stage.

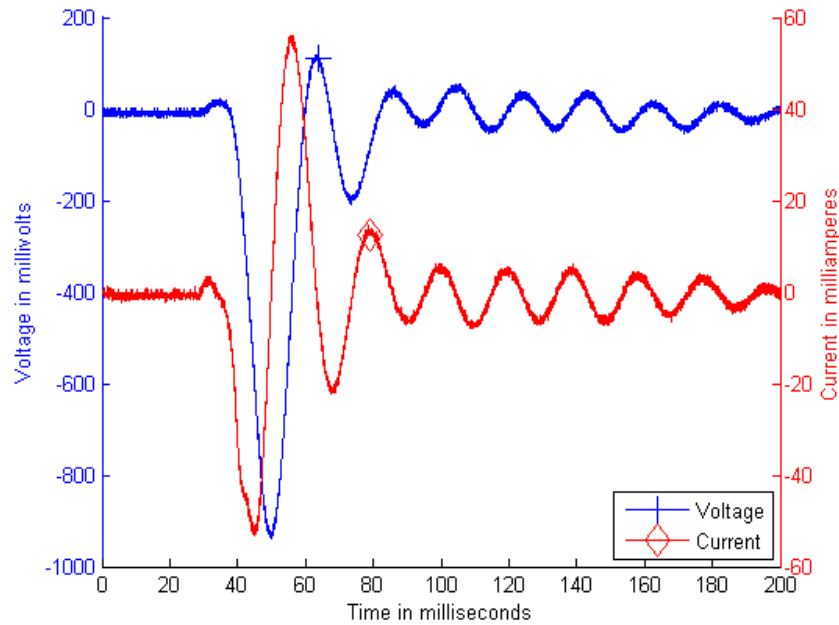


Figure 32. Release Stage Voltage and Current Generated Across Capacitor Terminals.

From Lenz's law, this correlates to current that behaves inversely to the compression current. Considering Faraday's law, we see a similar inverse

relationship in the voltage when comparing to compression. The voltage and current data in Figure 29 and Figure 32 confirm these expectations. The power generated during the release stage is shown in Figure 33.

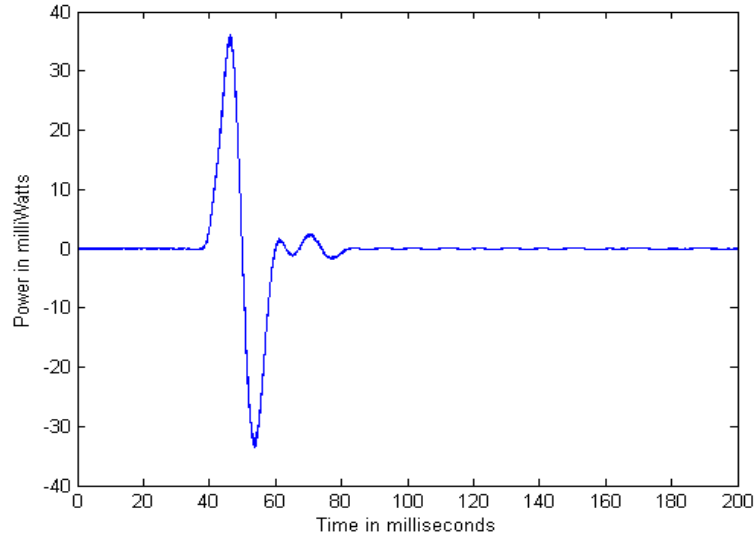


Figure 33. Release Stage Power Generated Across Capacitor Terminals.

The power increases as the capacitor charges and then becomes negative as the current reverses polarity, discharging the capacitor immediately. The subsequent energy data is shown in Figure 34. Given Equation (3.1), the energy in a capacitor is expected to remain positive regardless of the polarity of the voltage being considered. From this equation, a peak minimum voltage of negative 0.932 V while using the same 459 μF capacitor yields a peak energy of approximately 0.2 mJ. This value is confirmed by the data shown in Figure 34.

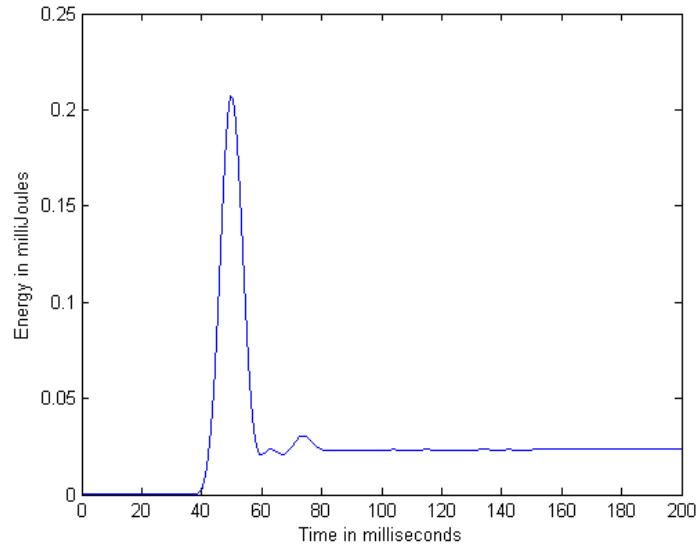


Figure 34. Release Stage Energy Generated Across Capacitor Terminals.

From the data collected during the compression and release stages, it can be seen that very little energy if any is actually being stored in the capacitor for a substantial amount of time. Changes in the polarity of the current related to the direction of change in the magnetic flux in the circuit cause the capacitor to charge and then discharge immediately. This correlates to a positive power spike during charging followed by a successive negative power spike during discharge. As a result, the net energy stored in the capacitor is close to nothing in this configuration.

3. Half-Wave Rectifier

In order to improve the amount of energy being stored in the capacitor, the half-wave rectifier circuit shown in Figure 20 was configured. The same tests for compression and release stages conducted with the single capacitor were then repeated and the results analyzed. The same 460 μF capacitor was used in the rectifier circuit, and the current probe was placed in the same position. The test circuit setup is shown in Figure 35.

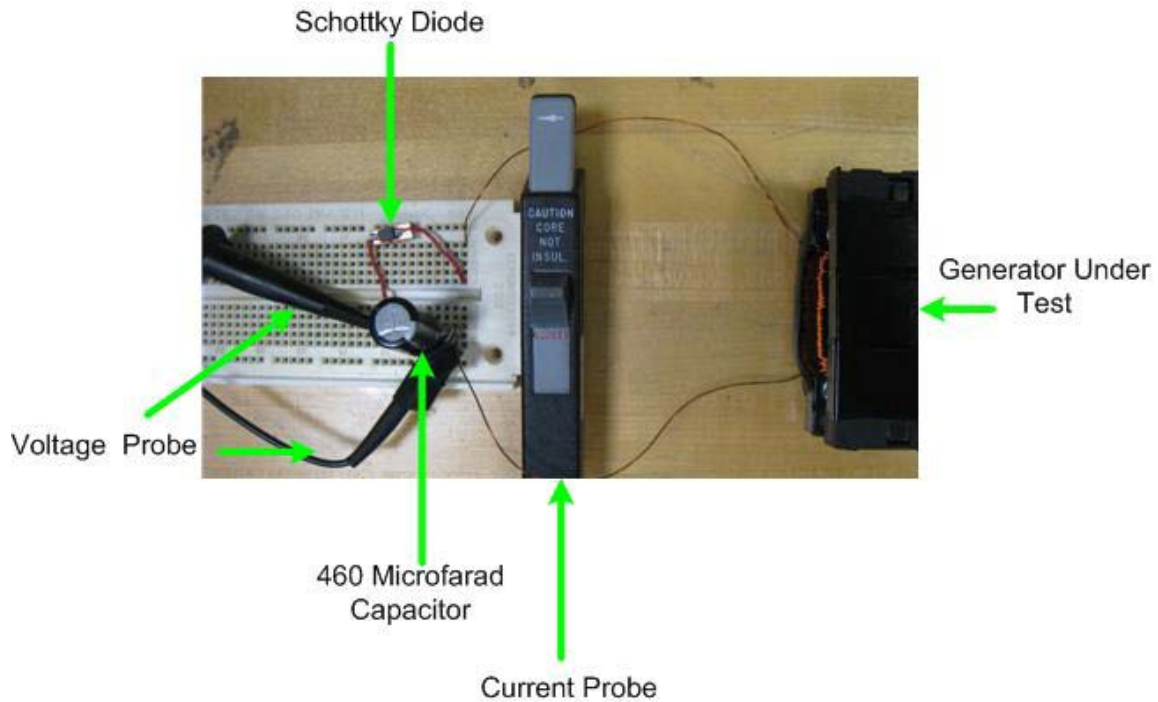


Figure 35. Half-Wave Rectifier Test Circuit Setup.

a. Compression Stage

The voltage and current data collected during the compression stage is shown in Figure 36. The rectifier circuit is expected to limit the flow of current in one direction, only eliminating the immediate discharge of the capacitor experienced in the previous tests.

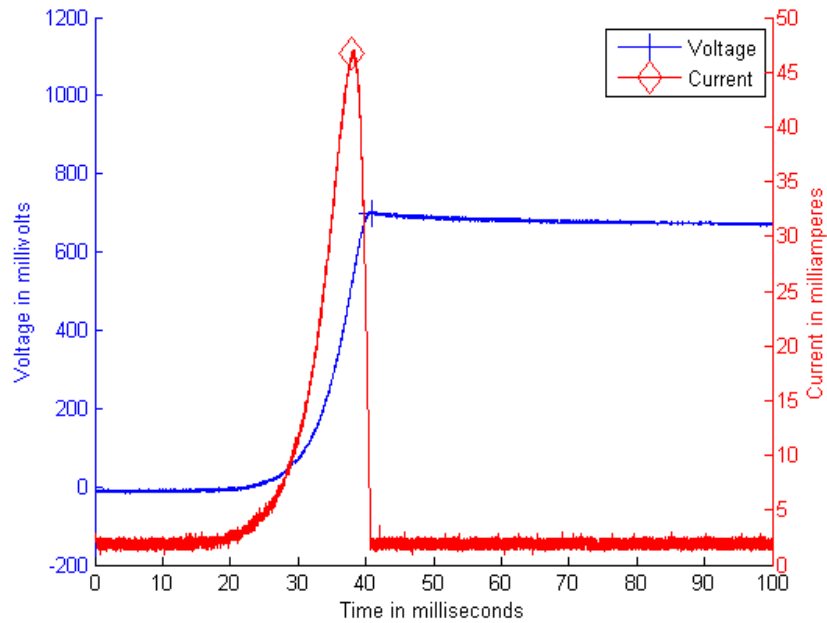


Figure 36. Compression Stage Voltage and Current Generated Across Capacitor Terminals.

The current behavior shown in Figure 36 confirms the current limited to flow in one direction only. As a result, the capacitor voltage charges and then maintains a positive charge for the remainder of the test period. The power generated plot shown in Figure 37 confirms power generation in the positive direction only. As a result, a net positive energy is experienced by the capacitor shown in Figure 38.

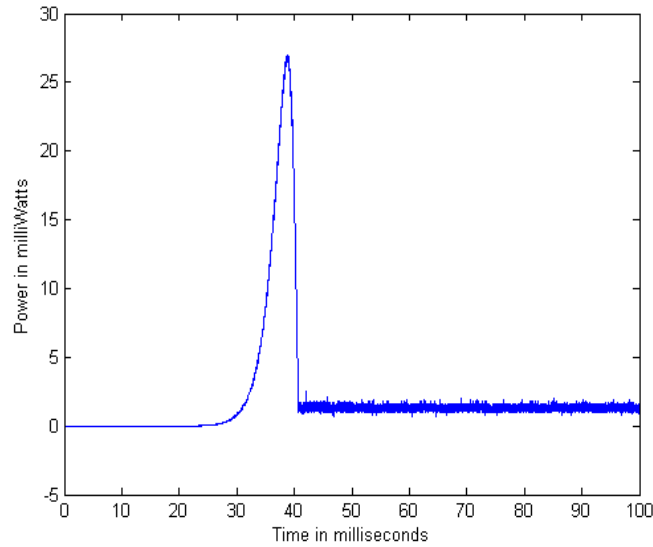


Figure 37. Compression Stage Power Generated Across Capacitor Terminals.

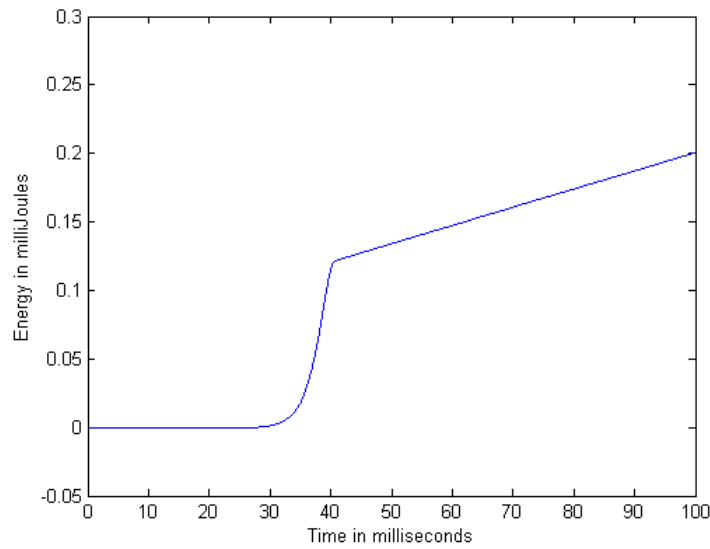


Figure 38. Compression Stage Energy Generated Across Capacitor Terminals.

b. Release Stage

To test the release stroke, the same half-wave rectifier was used as in the compression stage test except that the diode's cathode and anode were reversed. By flipping the diode, current is allowed to flow in the direction

opposite to that of the compression stage. The voltage and current probes were left in the same positions as the previous test. The resulting voltage and current data collected is shown in Figure 39.

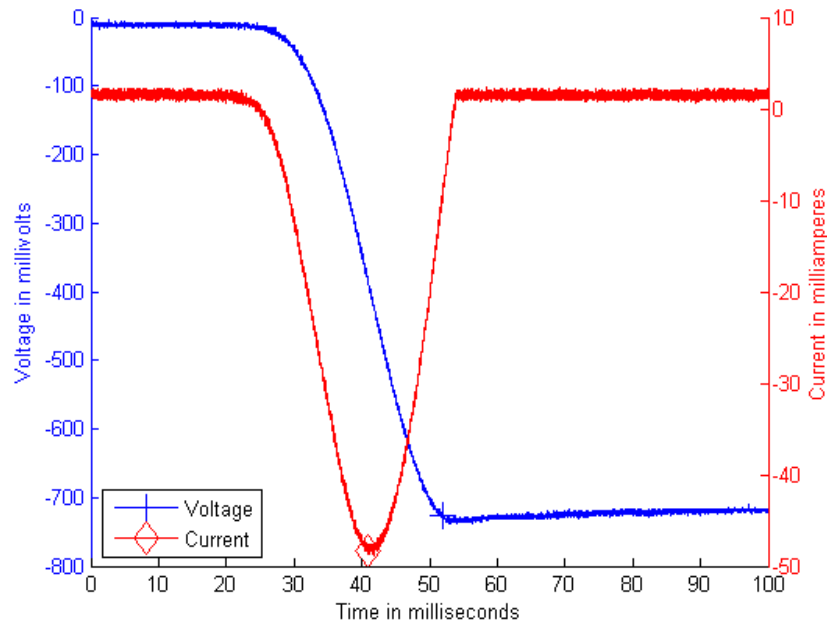


Figure 39. Release Stage Voltage and Current Generated Across Capacitor Terminals.

Similar to the compression stage, current is allowed to flow in one direction only, which is confirmed in the current plot. Since the current and voltage probes were left in the same positions, both result in negative values. Similar to the compression stage, the voltage decreases to a minimum value during charging of the capacitor and then maintains a minimum charge throughout the remaining duration of the test. Since the power generated is the product of voltage and current, a positive power spike is seen during the release of the device. This power surge is shown in Figure 33.

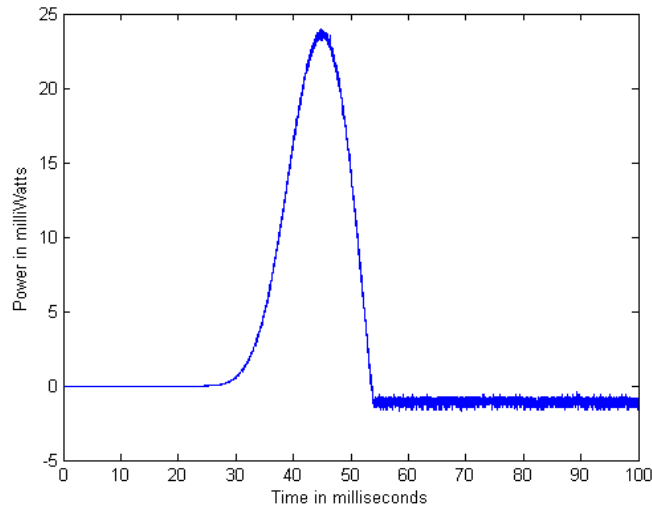


Figure 40. Release Stage Power Generated Across Capacitor Terminals.

The energy stored in the capacitor is shown in Figure 41. From the capacitor energy equation, the energy stored is expected to be positive even though the voltage measured is a negative value. This positive energy storage is confirmed in the energy plot below.

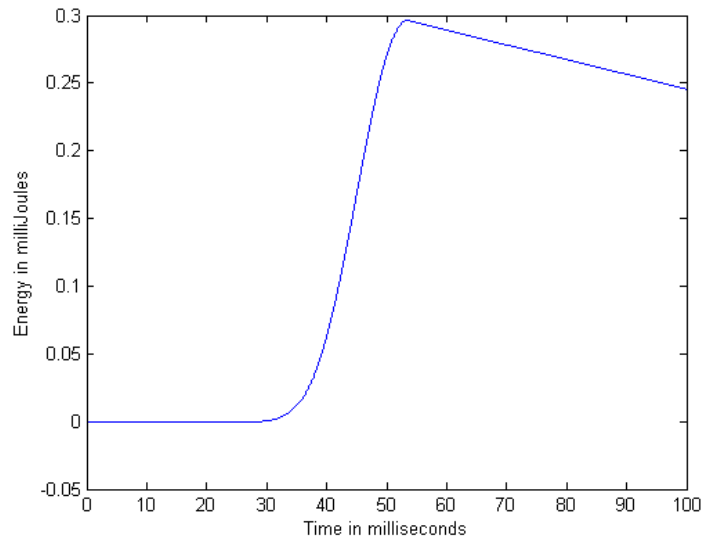


Figure 41. Release Stage Energy Generated Across Capacitor Terminals.

From the test data use, of the half-wave rectifier circuit demonstrates the creation and storage of electrical energy in the capacitor.

Depending on the orientation of the diode in the circuit, we see that energy can be stored from either compression or release of the generator, but not both stages simultaneously.

4. Doubling Circuit

In order to further improve the efficiency of energy storage over the half-wave rectifier circuit, the doubling circuit shown in Figure 21 was configured and tested. The half-wave rectifier limits current flow in only one direction, taking advantage of either the compression or release stage, but not both. The doubling circuit configuration should theoretically take advantage of both the compression and release stages and store energy in two separate capacitors for use. To test this, circuit, the voltage measurement is taken between the positive terminal of C_1 and the negative terminal of C_2 to determine the total voltage potential across both capacitors in series. Two current probes are used to verify current flow through each capacitor at separate times during the compression and release stage of the full stroke. One current probe is positioned at the anode of D_1 and one is positioned at the cathode of D_2 . To see the effects of both the compression and release together, a full-stroke test was conducted. The test circuit setup for the doubling circuit is shown in Figure 42.

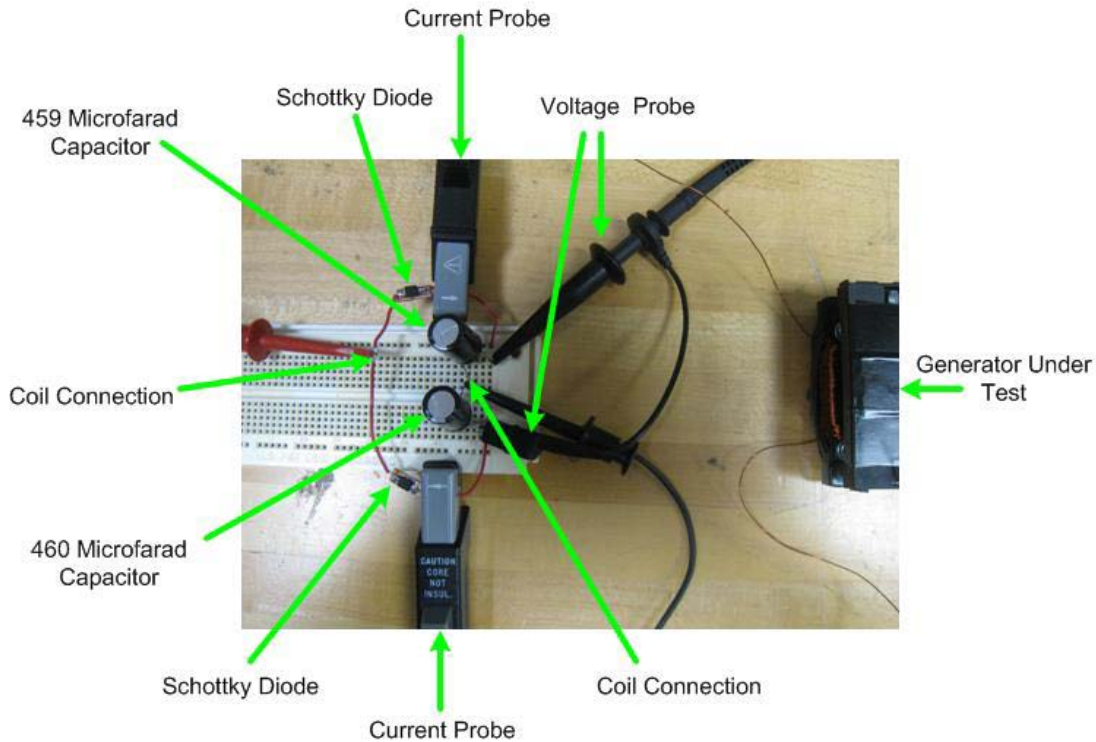


Figure 42. Doubling Circuit Test Configuration

a. Full-Stroke Test

The results of the voltage and current analysis of the full-stroke test is shown in Figure 43. The currents through the capacitors are tested separately to verify that current is being rectified in the intended manner of the doubling circuit. The doubling circuit is expected to allow current flow through one capacitor during the compression stage and the other capacitor during the release stage. The resulting data, shown in Figure 43, confirms this behavior where current flows through C_1 during compression only, and current flows through C_2 during release only. Two distinct voltage events are also expected, coinciding with the compression and release of the generator. From the voltage data, two charging events are clearly illustrated.

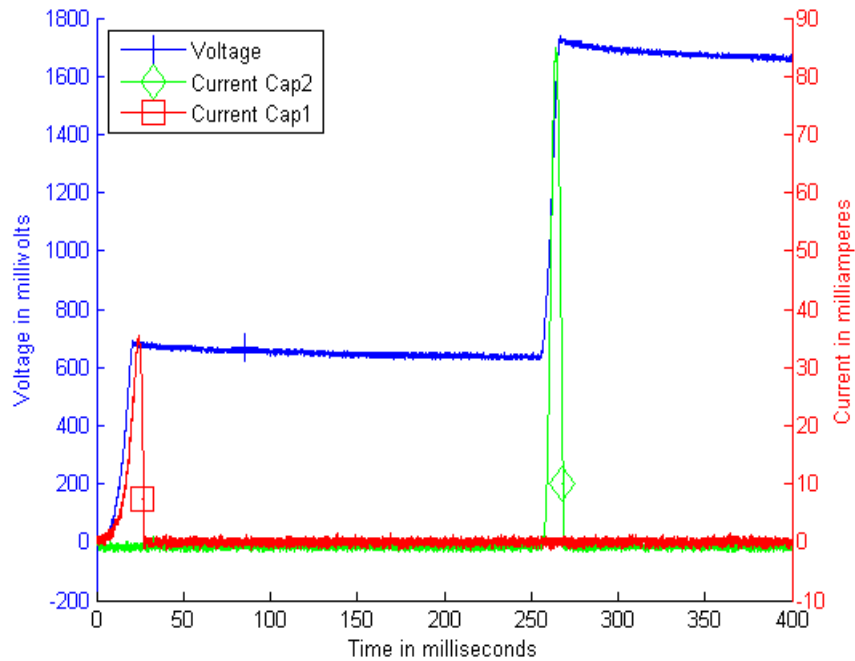


Figure 43. Full-Stroke Voltage and Current Generated Across Both Capacitors.

To obtain a plot of the power across the capacitor network, the product of the voltage and the summation of the two capacitor currents was analyzed. This power plot is shown in Figure 44. Integration of the power with respect to time results in the energy stored in the capacitor network shown in Figure 45.

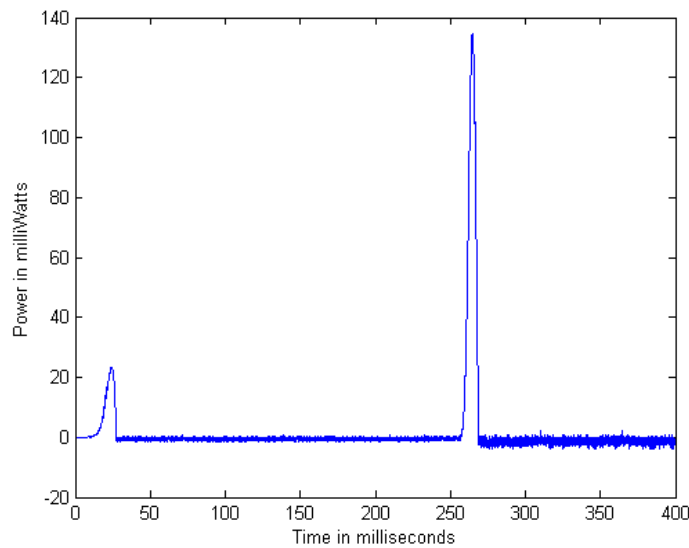


Figure 44. Full-Stroke Power Generated Across Both Capacitors.

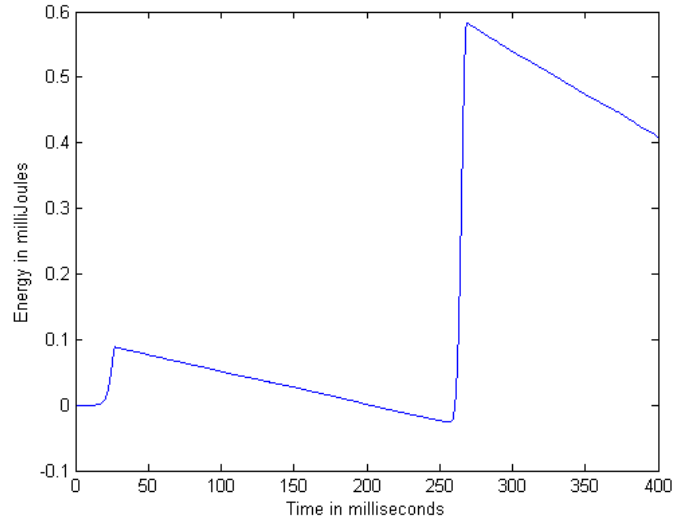


Figure 45. Full-Stroke Energy Generated Across Both Capacitors

From the power plot, it can be seen that nearly five times as much peak power is generated during the release stage than in the compression stage. Additionally, the energy stored in the circuit increases much higher during the release stage.

D. CHAPTER SUMMARY

This chapter detailed the construction of the generator prototype and subsequent testing of the device to verify its operation. The inductance of the generator coil is tested through the full displacement of the device, demonstrating the ferrite cores operation in saturation. The voltage, current, power and energy of the generator were compared through different stroke stages and three different energy storage configurations. In the next chapter, a computer simulation modeling the electromechanical energy conversion of the generator design will be discussed.

THIS PAGE INTENTIONALLY LEFT BLANK

IV. COMPUTER SIMULATION

Modeling of the generator operation was done utilizing the EM system design and the theory of operation discussed in Chapter II. This simulation was not used as a design aid for predicting generator performance but was created in parallel with the prototype. The goal of the simulation was to model general behavior of the system for use in perfecting future designs and prototypes

A. SIMULINK

The computer simulation of the generator was done using the SIMULINK simulation and model-based design software in MATLAB™. A model of an existing elementary electromechanical system incorporating a second-order spring damping system was modified to fit the generator design. This model relies on Newton's Law of Motion, applied in Equation (2.12), to balance the forces present in the system. The inductance range of operation for the generator was implemented using a cubic polynomial estimation of the inductance data measured in Figure 24. A change in flux in the system is modeled from the load flux in Equation (2.31) and a model of the coupling field energy and EMF is based on Equation (2.39). The SIMULINK block model diagram is shown in Appendix C.

B. RESULTS

The test of the generator simulation assumed a user conducting a full-stroke test with a 470 μF single capacitor as the storage element in the EM system. A force of 100 N was applied to the generator from the user and then released, causing the system displacement to go from an equilibrium position to minimum displacement and then back to equilibrium. During the application of force, we expect the inductance of the coil to follow the cubic polynomial model of the actual measured inductance values. The force application, system displacement and inductance of the simulated system are shown in Figure 46.

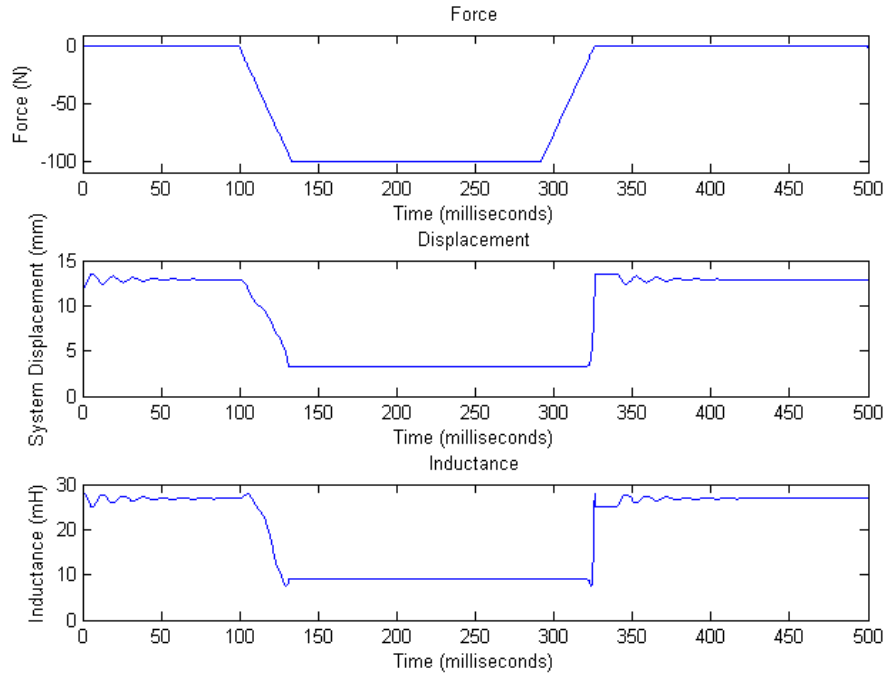


Figure 46. Computer Simulated Force, Displacement and Inductance.

The force application is in the negative direction in the simulation to correlate to the displacement of the system defined as being positive to the right in the EM system, shown in Figure 5. As a result, a negative force is required to close the generator. As seen in the displacement data, when the force is applied, the displacement quickly decreases to the minimum displacement of 3.345 mm and returns to an equilibrium position once the force is removed. Some damping of the system is also illustrated in the displacement data by oscillations prior to reaching a steady-state equilibrium displacement. The inductance follows closely the values expected from the displacements measured in Figure 24, with some variations at the maximum and minimum displacements due to the error of the measured inductance values and the polynomial equation used to model them.

The voltage and current response of the system was modeled to simulate the full-stroke response of the system, and is shown in Figure 47.

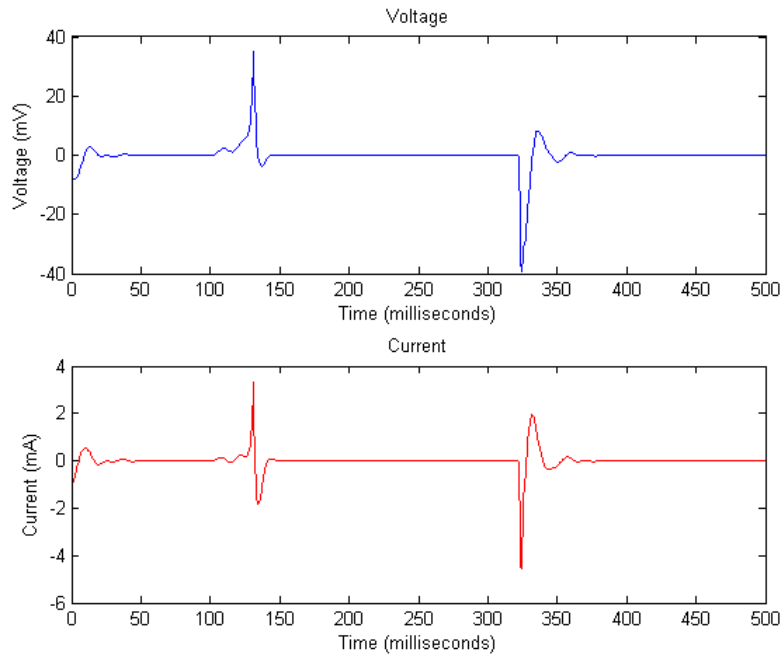


Figure 47. Simulated Voltage and Current Response.

The voltage and current simulation data clearly shows two events occur and correlate to the times when the force is exerted and relaxed in the system. This same behavior is seen in the experimental measurements in Figure 26. The two events in the simulation are intended to represent the compression and release stages of the full stroke of the generated. The simulated compression stage is shown in Figure 48.

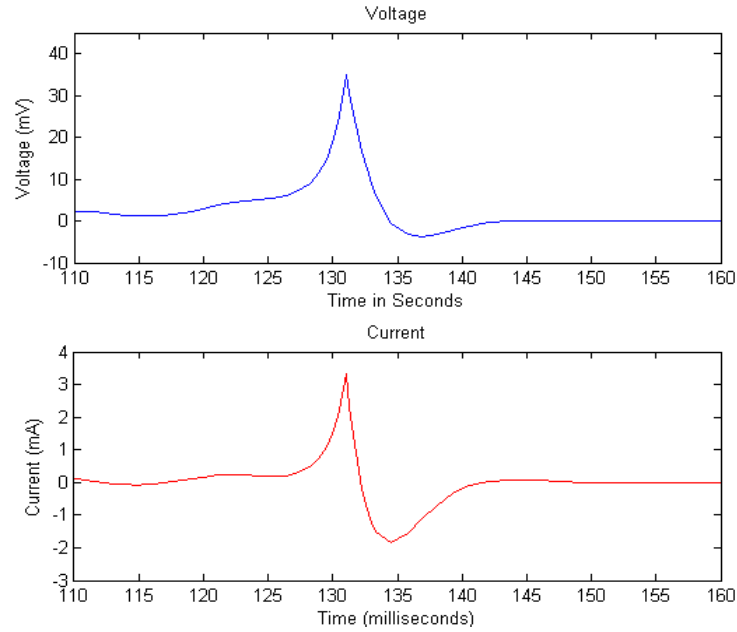


Figure 48. Simulated Voltage and Current Data During Compression Stage.

The simulated compression stage voltage and current exhibit similar behavior to the experimental compression stage data shown in Figure 29. During the experimental compression stage, we see that voltage and current values rise when the force is exerted on the generator, charging the capacitor to a peak voltage and then discharging immediately. The simulation behaves in a similar manner, illustrating the positive current followed immediately by a reverse in current polarity and subsequent discharge of the capacitor voltage.

The release stage simulation data is shown in Figure 49. The simulated release stage voltage and current also exhibit similar behavior to the experimental data shown in Figure 32. The experimental release stage voltage and current values fall when the force is exerted on the generator, charging the capacitor to a minimum voltage and then discharging. The simulation behaves in a similar manner, exhibiting a negative current followed immediately by a reverse in current polarity to positive discharging the voltage stored in the capacitor.

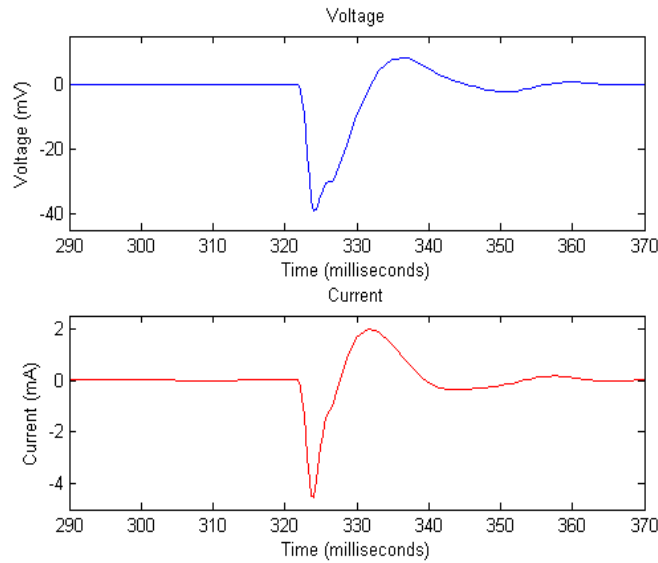


Figure 49. Simulated Voltage and Current Data During Release Stage.

Although the behavior of the voltage and simulation data concurs with the experimental data taken, the magnitudes of the voltage and current data are much lower than the experimental values measured.

The power generated during simulation is illustrated in Figure 50, showing two distinct events with large positive power generation and small negative power elements. The second event correlating to the release stage models a much higher power output during release, which is confirmed through experimental data shown in Figure 27.

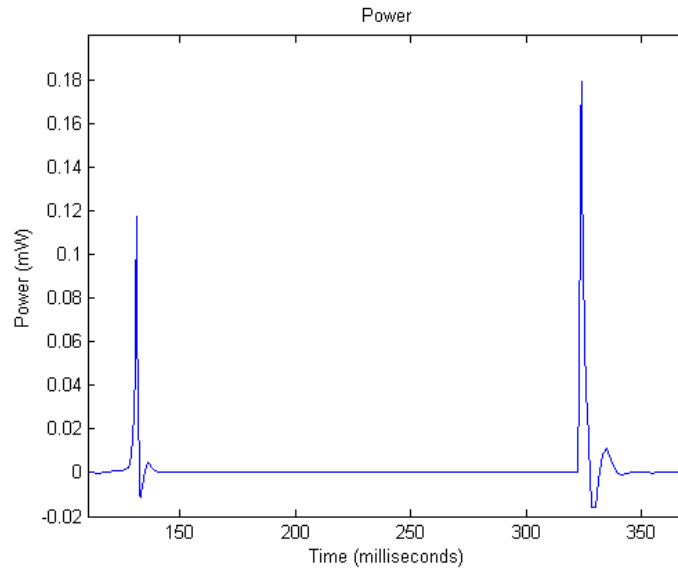


Figure 50. Simulated Power Generation During Full-Stroke.

The power generated during experimental data experienced much higher negative power spikes immediately following the positive power spikes. The negative power elements show up in the model but are much lower in magnitude than experimental measurements.

The inconsistencies in the power generated during the simulation also translate to different results in the simulated energy storage. In the experimental measurements, the large negative power matched the positive power generated and nearly no net energy storage was measured. The lack of a matching negative power generated in the simulation leads to an electrical energy stored that was not present in the experimental measurements. The simulated electrical energy exhibits a negative polarity and is shown in Figure 51. This concurs with electrical energy leaving the coupling field as defined in the energy balance diagram shown in Figure 4.

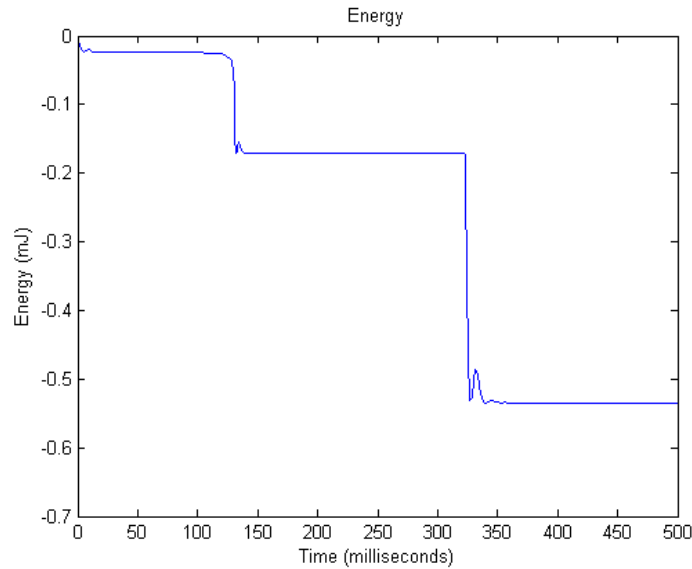


Figure 51. Simulated Energy During Full Stroke.

C. CHAPTER SUMMARY

This chapter detailed the computer simulation of the generator created using the SIMULINK simulation environment in MATLAB™. The model created was able to exhibit some general behavior characteristics matching experimental testing of the generator using only a single capacitor connected to the generator coil. The voltage and current behavior during a simulated force exerted on the generator performed similarly to the experimental measurements but was much lower in magnitude than experimental data measurements. The simulated power output of the generator experienced positive power spike events similar to that of the experimental data; however, some inconsistencies with the negative power measurements were seen. This, in turn, resulted in some energy being stored in the simulation, where there was little or no energy storage experimentally. Consequently, the computer simulation model requires additional adjustments to fully model all aspects of the generator.

THIS PAGE INTENTIONALLY LEFT BLANK

V. CONCLUSIONS AND RECOMMENDATIONS

A. CONCLUSION

A miniature electromechanical generator utilizing human motion provided by the user was successfully designed, constructed and tested. The system was designed incorporating EM system and magnetic circuit theory and realized using inexpensive and easily obtainable materials. Successful operation of the generator was verified by experimental results, demonstrating the charging of capacitors in two separate rectification circuits. These results achieved a peak voltage potential of more than 1.7 V stored across two capacitors in a single generator stroke. Computer modeling of the device was able to exhibit some general voltage and current behavior of the system.

B. RECOMMENDED FURTHER RESEARCH

The effect of saturating the ferrite cores warrants additional investigation into how this may be utilized better or avoided for better performance in the generator. In relation to saturation, the ferrite cores used have a relatively low initial permeability compared to other higher quality core materials with higher saturation points. Higher permeability cores may show performance improvements in the system but are more difficult and much more expensive than the ferrite cores used. Planar I-shaped cores used as matching bases to E-shaped cores could be found in similar dimensions and should be tested in the generator design to see if significant performance improvements can be made.

Application-specific testing where energy is generated, stored and used in an electronic device should be tested to see what potential and limitations the device has for operating ultra-low low power devices. The generator output can be further conditioned to better match the power requirements of such devices.

Computer modeling of the system only exhibits general behavioral similarities to the experimental voltage and current experienced. This can be improved by additional measurements using a magnetic flux meter and

conducting controlled force testing of the mechanical input to the device to map its behavior more closely. Additionally, finite element analysis should be conducted to predict the permanent magnet behavior more accurately within the system.

APPENDIX A. MATLAB CODE FOR INDUCTANCE PROFILE GENERATION

```
x_meas=.001.*[.17 .36 .56 .74 .94 1.13 1.33 1.53 1.73 1.92 2.13 2.32
2.52 2.72 2.91 3.09 3.30 3.49 3.70 3.88 4.07 4.26 4.47 4.66 4.86 5.07
5.26 5.45 5.65 5.85 6.03 6.24 6.43 6.62 6.81 6.9 7.15 7.35 7.55 7.74
7.93 8.12 8.33 8.51 8.70 8.90 9.10 9.29 9.49 9.69 9.87 10.05 10.15];
L_meas=.001.*[8.81 8.31 8.14 8.06 8.00 7.85 7.85 7.89 7.92 8.00 8.03
8.24 8.45 8.54 8.98 9.40 9.81 10.25 10.95 11.72 12.78 14.02 15.34 16.76
17.40 18.20 19.28 20.19 21.09 21.82 22.58 23.15 23.71 24.28 24.67 25.09
25.40 25.74 25.97 26.20 26.39 26.53 26.63 26.73 26.80 26.86 26.91 26.94
26.95 26.96 26.97 27.01 27.37];
x_meas=x_meas+.003175 %Min air gap is .003450m due to magnets
and one thickness of electrical tape insulator
plot(x_meas*1000,L_meas*1000);
xlabel('System Displacement in millimeters');
ylabel('Inductance in millihenries');
title('Inductance vs. System Displacement');
```

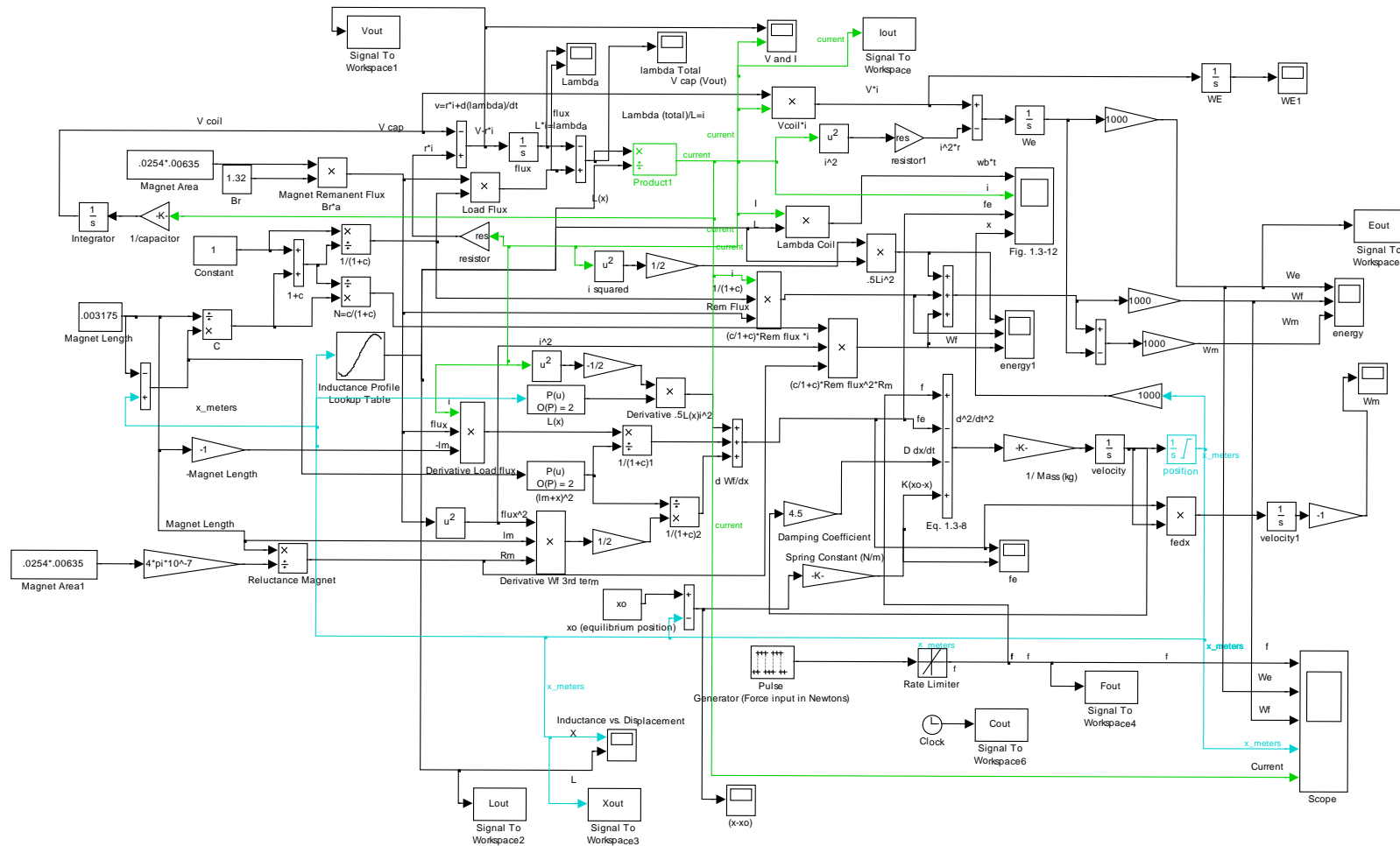
THIS PAGE INTENTIONALLY LEFT BLANK

APPENDIX B. MATLAB CODE FOR DATA ANALYSIS

```
%Import data into Matlab first
%Voltage and Current Data Plotted separately and then together
SampleLength=.400; %Horizontal time per/div * 10
time = [0+(SampleLength/10000):(SampleLength/10000):SampleLength];
%convert time scale of data for 10,000 data points
IprobeVar=1; %Amps/Div setting on Probe divided by 10mA/Div
Current=1*IprobeVar*ImportCurrentDataCh1(1:10000,2); %Adjust for
amplitude of the current probe
plot(time*1000,Current,'Color','r','DisplayName','Current');
xlabel('Time in milliseconds');
ylabel('milliamps');
title('Current');
Voltage=ImportCurrentDataCh2(1:10000,2);
plot(time*1000,Voltage,'DisplayName','Voltage');
xlabel('Time in milliseconds');
ylabel('Volts');
title('Voltage');
figure
hold on
plot(x1,y1,'Color','b','MarkerSize',12,'Marker','+','DisplayName','Volt
age'); % Dual axes marker position for voltage
plot(x2,y2,'Color','g','MarkerSize',12,'Marker','diamond','DisplayName'
,'Current'); %Dual axes marker position for voltage
legend('Location','NorthWest'); %Legend location
hl1 = line(time*1000,1000*Voltage,'Color','b','DisplayName','Voltage');
ax1 = gca;
ylabel('Voltage in millivolts');
set(ax1,'XColor','k','YColor','b')
ax2 =
axes('Position',get(ax1,'Position'),'XAxisLocation','bottom','YAxisLoca
tion','right','Color','none','XColor','k','YColor','r');
hl2 =
line(time*1000,1000*Current,'Color','g','Parent',ax2,'DisplayName','Cur
rent1');
ylabel('Current in milliamperes');
xlabel('Time in milliseconds');
hold off
%% Power and Energy Data
figure
Power=Voltage.*Current; % P=V*I
plot(time*1000,Power*1000);
xlabel('Time in milliseconds');
ylabel('Power in milliWatts');
title('Power');
figure
Energy=cumtrapz(time,Power); % Energy = integral of Power w/ respect to
time
plot(time*1000,Energy*1000);
xlabel('Time in milliseconds');
ylabel('Energy in milliJoules');
title('Energy');
```

THIS PAGE INTENTIONALLY LEFT BLANK

APPENDIX C. SIMULINK MODEL



THIS PAGE INTENTIONALLY LEFT BLANK

APPENDIX D. MATLAB CODE FOR SIMULATION DATA

```
%Run Simulation of Simulink Model first
% Force, Displacement, and Inductance
time=Cout;
figure(1)
subplot(3,1,1)
plot(Cout*1000,Fout, 'Color', 'b', 'DisplayName', 'Force');
xlabel('Time (milliseconds)');
ylabel('Force (N)');
title('Force');
subplot(3,1,2)
plot(Cout*1000,Xout*1000, 'Color', 'b', 'DisplayName', 'displacement');
xlabel('Time (milliseconds)');
ylabel('System Displacement (mm)');
title('Displacement');
subplot(3,1,3)
plot(Cout*1000,Lout*1000, 'Color', 'b', 'DisplayName', 'Inductance');
xlabel('Time (milliseconds)');
ylabel('Inductance (mH)');
title('Inductance');
%% VI Data
Current=Iout;           %Adjust for amplitude of the current probe, probe
set at .5Amps/div with ten turns of wire around the probe
Voltage=Vout;
figure(2);
subplot(2,1,1)
plot(time*1000,Voltage*1000, 'Color', 'b', 'DisplayName', 'Voltage');
xlabel('Time (milliseconds)');
ylabel('Voltage (mV)');
title('Voltage');
Voltage=Vout;
subplot(2,1,2)
plot(time*1000,Current*1000, 'Color', 'r', 'DisplayName', 'Current');
xlabel('Time (milliseconds)');
ylabel('Current (mA)');
title('Current');
%% Compression Stage
figure(3);
subplot(2,1,1)
plot(time*1000,1000*Voltage, 'Color', 'b', 'DisplayName', 'Voltage');
axis([110 160 -10 45])
xlabel('Time in Seconds');
ylabel('Voltage (mV)');
title('Voltage');
subplot(2,1,2)
plot(time*1000,1000*Current, 'Color', 'r', 'DisplayName', 'Current');
axis([110 160 -3 4])
xlabel('Time (milliseconds)');
ylabel('Current (mA)');
title('Current');
%% Release Stage
figure(4);
```

```

subplot(2,1,1)
plot(time*1000,1000*Voltage,'Color','b','DisplayName','Voltage');
axis([290 370 -45 15])
xlabel('Time (milliseconds)');
ylabel('Voltage (mV)');
title('Voltage');
subplot(2,1,2)
plot(time*1000,1000*Current,'Color','r','DisplayName','Current');
axis([290 370 -5 2.5])
xlabel('Time (milliseconds)');
ylabel('Current (mA)');
title('Current');
%% Power
figure(5)
plot(time*1000,Voltage.*Current*1000,'Color','b','DisplayName','Power')
;
axis([110 370 -.02 .2])
xlabel('Time (milliseconds)');
ylabel('Power (mW)');
title('Power');
%% Energy
figure(6)
plot(time*1000,Eout*1000,'Color','b','DisplayName','Energy');
%axis([150 400 -.02 .15])
xlabel('Time (milliseconds)');
ylabel('Energy (mJ)');
title('Energy');

```

LIST OF REFERENCES

- [1] "Defense infrastructure: Department of Defense renewable energy initiatives," *Briefing for the Committees on Armed Services, United States Senate and House of Representatives*. Government Accountability Office, 26 April 2010.
- [2] R. E. Mabus, "Energy awareness message," 30 October 2009. <http://www.navy.mil/navydata/people/secnav/Mabus/Message/Energy%20Message%20ALNAV.pdf> (accessed September 8, 2010).
- [3] T. O. Kiper, A. E. Hughley, and M. R. McClellan, "Batteries on the battlefield: Developing a methodology to estimate the fully burdened cost of batteries in the Department of Defense," Master's thesis, Naval Postgraduate School, 2010.
- [4] D. P. Arnold, "Review of microscale magnetic power generation," *IEEE Trans. Magn.*, vol. 43, no. 11, pp. 3940–3951, Nov. 2007.
- [5] A. S. Holmes, G. Hong, and K. R. Pullen, "Axial-flux permanent magnet machines for micropower generation," *J. Microelectromech. Syst.*, vol. 14, no. 1 pp. 54–62. Feb. 2005.
- [6] J. Peirs, D. Reynaerts, and F. Verplaetsen, "A microturbine for electric power generation," *Sens. Actuators A*, vol. 114, pp. 86–93, 2004.
- [7] H. Raisigel, O. Cugat, and J. Delamare, "Permanent magnet planar micro-generators," *Sens. Actuators A*, vol. 130–131, pp. 438–444, Aug. 2006.
- [8] R. Amirtharaja, and A. P. Chandrakasan, "Self-powered signal processing using vibration-based power generation," *IEEE J. Solid-State Circuits*, vol. 33, no. 5, pp.687–695, May 1998.
- [9] Ferro Solutions, VEH-460 Energy Harvester Data Sheet. http://www.ferrosi.com/files/VEH460_May09.pdf (accessed September 10, 2010).
- [10] F. T. Ulaby, *Fundamentals of Applied Electromagnetics*, 5th Ed. NJ: Prentice Hall, 2007.
- [11] P. C. Krause, O. Wasynczuk and S. D. Sudhoff, *Analysis of Electric Machinery and Drive Systems*. John Wiley and Sons, 2002.
- [12] Laird Technologies, 28S2001-0M0 Split Ferrite Core, http://media.digikey.com/photos/Steward%20Photos/28S2001-0M0%20_sml.jpg (accessed August 25, 2010).

- [13] Laird Technologies, 28S2001-2A2 Split Ferrite Core, http://media.digikey.com/photos/Steward%20Photos/28S2001-2A2_sml.jpg (accessed August 25, 2010).
- [14] "Neodymium magnet information," KJ Magnetics, Inc. <http://www.kjmagnetics.com/neomaginfo.asp> (accessed August 30, 2010).
- [15] "Magnetization direction for neodymium magnets," <http://www.kjmagnetics.com/images/magdir.block.short.png> (accessed August 30, 2010).
- [16] "Neodymium block magnet BX042," <http://www.kjmagnetics.com/prodimages/BX042L.jpg> (accessed August 31, 2010).
- [17] D. Meeker, "Circuit model of a uniformly magnetized cylindrical permanent magnet," <http://www.femm.info/Archives/misc/BarMagnet.pdf> (accessed August 30, 2010).
- [18] "Rare earth magnet basics," Shin-Etsu Chemical Co. Ltd., <http://www.shinetsu-rare-earth-magnet.jp/e/design/> (accessed August 25, 2010).
- [19] "Permanent magnets," <http://www.rare-earth-magnets.com/images2/00303.jpg> (accessed August 25, 2010).
- [20] Vishay Intertechnology, 10BQ015 Schottky Rectifier Data Sheet.
- [21] P.C. Krause and O. Wasynczuk, *Electromechanical Motion Devices*. New York: McGraw-Hill, 1989.
- [22] R. M. Bozorth, *Ferromagnetism*. New York: IEEE Press, 1951.
- [23] G. G. Orenchak, "Specify saturation properties of ferrite cores to prevent field failure," http://www.elnamagnetics.com/wp-content/uploads/library/TSC-Ferrite-International/Specify_Saturation_Properties_of_Ferrite_Cores_to_Prevent_Field_Failure.pdf (accessed September 1, 2010).
- [24] J. W. Nilsson and S. A. Reidel, *Electronic Circuits*, 8th Ed. NJ: Prentice Hall, 2008.

INITIAL DISTRIBUTION LIST

1. Defense Technical Information Center
Ft. Belvoir, Virginia
2. Dudley Knox Library
Naval Postgraduate School
Monterey, California
3. Dr. R. Clark Robertson
Naval Postgraduate School
Monterey, California
4. Dr. Alexander L. Julian
Naval Postgraduate School
Monterey, California
5. Dr. Giovanna Oriti
Naval Postgraduate School
Monterey, California
6. LT Nicholas G. Hoffman
United States Navy
Monterey, California